Relative influences of multiple sources of uncertainty on cumulative and incremental tree-ring-derived aboveground biomass estimates

Relative influences of multiple sources of uncertainty on cumulative and incremental tree-ring-derived aboveground biomass estimates

In preparation for: Trees: Structure and Function

Authors: M. Ross Alexander[1,2], Christine R. Rollinson[3], Flurin Babst[1],[4,5], Valerie Trouet[1], David J.P. Moore[2]

[1] The Laboratory of Tree-Ring Research, The University of Arizona, 1215 E. Lowell St. Tucson, AZ 85721

[2] School of Natural Resources and the Environment, The University of Arizona, 1064 E. Lowell St. Tucson, AZ 85721

[3] Department of Earth and Environment, Boston University, 685 Commonwealth Ave, Room 130 Boston, MA 02215

[4] Dendroclimatology group, Swiss Federal Research Institute WSL, Zürcherstrasse 111, CH-8903 Birmensdorf, Switzerland

[5] W. Szafer Institute of Botany, Polish Academy of Sciences, ul. Lubicz 46, 31-512 Krakow, Poland

Abstract

How forest growth responds to climate change will impact the global carbon cycle. The sensitivity of tree growth and thus forest productivity to climate can be inferred from tree-ring increments, but individual tree responses may differ from the overall forest response. Tree-ring data have also been used to estimate interannual variability in aboveground biomass, but a shortage of robust uncertainty estimates often limits comparisons with other measurements of the carbon cycle across variable ecological settings. Here we identify and quantify four important sources of uncertainty that affect tree-ring based aboveground biomass estimates: subsampling, allometry, forest density (sampling), and mortality. In addition, we investigate whether transforming rings widths into biomass affects the underlying growth-climate relationships at two coniferous forests located in the Valles Caldera in northern New Mexico.

Allometric and mortality sources of uncertainty contributed most (34-57% and 24-42%, respectively) and subsampling uncertainty least (7-8%) to the total uncertainty for cumulative biomass estimates. Subsampling uncertainty, however, was the largest source of uncertainty for year-to-year variations in biomass estimates, and its large contribution indicates that between-tree growth variability remains influential to changes in year-to-year biomass estimates for a stand. The effect of the large contribution of the subsampling uncertainty is reflected by the different climate responses of large and small trees. Yet, the average influence of climate on tree growth persisted through the biomass transformation, and the biomass growth-climate relationship is comparable to that found in traditional climate reconstruction-oriented tree-ring chronologies. Including the uncertainties in estimates of aboveground biomass will aid

comparisons of biomass increment across disparate forests, as well as further the use of these data in vegetation modeling frameworks.

Keywords: Carbon Cycle, Aboveground biomass estimates, Uncertainty, Tree Rings, Growth-climate Relationships

Key Message

Growth-climate relationships are preserved when transforming tree-ring data to aboveground biomass estimates, the uncertainties of which are dominated by choice of allometric equation and mortality accounting in cumulative calculations and by subsampling in year-to-year estimates.

Introduction

Whether the biosphere will act as a source or sink of carbon in the next century depends in part on how forest ecosystems respond to changing climate conditions (Friedlingstein et al. 2006). Forests account for 30% of the terrestrial land area and store almost 45% of the terrestrial carbon (Bonan 2008). Evaluation of the sensitivity of carbon uptake to climate, however, is challenging. Direct manipulations of temperature and rainfall are typically limited to small stature ecosystems and short time scales (Shaver et al. 2000; Lu et al. 2012). In established forest ecosystems, we are limited to estimating carbon uptake in response to current or historical climate using methods such as forest inventories, eddy-covariance towers, or remote sensing. Estimates of forest carbon uptake from these sources are thus an important benchmark for land surface models (Beer et al 2010, Barr et al 2013). However, these datasets are only available for a fraction of the lifespan of trees, and the variance in temperature and rainfall recorded in these relatively short-term records are typically a poor sample of long-term oscillations in the climate system. Furthermore, harmonized continental- or global-scale products often rely on simplifying assumptions such as the use of global, non-species or site-specific allometric equations that complicate comparisons with field data.

Multi-century and even multi-millennial tree-ring chronologies detail the seasonal and annual climate variability experienced by temperate, boreal, and alpine trees over the course of their lifespan (Mann et al. 1998; Cook et al. 2004; Griffin et al. 2011; Williams et al. 2012; Belmecheri et al. 2015). For example, winter precipitation and summer temperature are the most influential growth factors for trees in semi-arid regions (Touchan et al. 2011; Brice et al.

2013; St. George and Ault 2014; St. George 2014) whereas forests in more mesic environments are most strongly influenced by summer precipitation (St. George et al. 2010; St. George 2014). Furthermore, tree-ring data have been useful in developing stand-level biomass reconstructions to investigate long-term trends in aboveground productivity, and specifically the interannual fluctuations of this large carbon pool as a result of changing environmental conditions (Graumlich et al. 1989; Babst et al. 2014b; Babst et al. 2014a; Dye et al. 2016).

There are, however, several limitations to using tree-ring records to infer climate sensitivities of carbon uptake. In most tree-ring analyses, the mean ring-width increment across multiple individuals is used to represent the growth at the site level (Hughes 2011). However, this method can ignore the individual tree-level variability that is ecologically-relevant and contributes to the stand-level growth response in each year. Factors such as tree size, competition, topography, and microclimate can cause different annual responses among individuals and may not be captured by sampling only the largest and oldest individuals at a site, as is common in many dendrochronological studies (Esper et al. 2008; Carnwath et al. 2012; Nehrbass-Ahles et al. 2014; Foster et al. 2016, Lenoir et al. 2017; Kovács et al. 2017). Furhtermore, increment cores are records of diameter growth and must be translated to carbon uptake through the use of derived allometric equations that translate linear growth to increments of stem volume and carbon content (Graumlich et al. 1989; Jenkins et al. 2004; Babst et al. 2014b; Babst et al. 2014a; Nehrbass-Ahles et al. 2014). Stand density can also affect biomass estimates. Traditional dendroclimatology sampling methods greatly overestimate the potential biomass on the landscape by only sampling the oldest or largest individuals (Nehrbass-Ahles et al. 2014). Not only does this potentially overestimate the biomass estimates, but it may

100 also influence our quantifications of how climate influences tree growth (Nehrbass-Ahles 2014).
101 Therefore, ecological sampling designs where all individuals in a fixed plot or a random sub-
102 sample are included have been implemented to estimate forest productivity (e.g. Davis et al.
103 2009; Babst et al. 2014b; Dye et al. 2016). Finally, trees that are on the landscape today do not
104 necessarily represent all trees that have contributed to biomass increment in the past. This
105 uncertainty increases as one goes further back in time, when less stand information is available
106 (Swetnam et al. 1999; Babst et al. 2014a; Nehrbass-Ahles et al. 2014). However, this fading
107 record and mortality estimates can be estimated using repeat censuses, but extended, multi-
108 decadal census datasets are rare (Biondi 1999; van Mantgem et al. 2009; Dye et al. 2016).
109 Without a proper accounting of these various sources of uncertainty surrounding biomass
110 estimates, the applicability of tree-ring data to data assimilation and vegetation modeling efforts
111 is restricted (Keenan et al. 2011). Ecosystem models are used to forecast how forests will
112 respond to future global changes and rely on empirical observations of biomass change for
113 benchmarking and structural improvements (Richardson et al. 2010). Here, we aim to evaluate
114 the climate sensitivity of tree growth and aboveground biomass increment in a semiarid forest in
115 the Southwest USA while accounting for uncertainty in the biomass estimates. Forests in semi-
116 arid regions are particularly sensitive to climate change, with small changes in climate and
117 growing conditions potentially resulting in large variability in carbon uptake (Poulter et al. 2014;
118 Ahlström et al. 2015). We estimate the uncertainty in tree-ring-based estimates of living
119 aboveground biomass increment for two semi-arid forests from 1980 through 2011 contributed
120 by (1) the selection of allometric equations (allometric uncertainty), (2) ability of sampled trees to
121 capture variability and patterns in annual growth increments of the forest (subsampling

uncertainty), (3) ability of sampling location to accurately capture overall mean forest density (sampling uncertainty), and (4) trends in tree mortality through time (mortality uncertainty). We then assess whether biomass transformations significantly alter the growth-climate relationship from that expressed by tree-ring chronologies.

Methods

Sampling design and site description

Two sites were sampled in the Valles Caldera National Preserve, one upper elevation and one lower elevation site, located in the Jemez Mountains of northern New Mexico. This semi-arid continental region experiences dry conditions in May and June and frequent pulses of monsoon moisture in July and August (Coop and Givnish 2007). The upper elevation site (Upper Site; 35.89N, 106.53W) has an elevation of 3049 m.a.s.l. and is composed of 97% Engelmann spruce (*Picea engelmanii* Parry ex Engelm.; PIEN) with the scattered Douglas fir (*Pseudotsuga menziesii* (Mirb.); PSME; Anderson-Teixeira et al. 2011). The Upper Site has a mean annual temperature of 3.1˚C and a mean precipitation of 667 mm per year (Anderson-Teixeira et al. 2011). The lower elevation site (Lower Site; 35.86N, 106.60W) is located at 2486 m.a.s.l., and is dominated by ponderosa pine (*Pinus ponderosa* Douglas ex C. Lawson; PIPO), with one *Populus tremuloides* Michx. individual. The mean annual temperature at the Lower Site is 6.3˚C and it receives on average 550 mm of precipitation annually (Anderson-Teixeira et al. 2011).

Previous, independent studies have generated aboveground biomass estimates for the Valles Caldera, but did not fully account for the different sources of uncertainty (Anderson-Teixeira et al 2011). Although our research is performed at the same site, we did not replicate

143 previously sampled locations and used a different sampling method. We established two plots of
144 576 m^2 at the Upper Site and one 576 m^2 and one 624m^2 at the Lower Site. The second plot at
145 the Lower Site was slightly larger to allow a similar number of stems to be sampled in both plots.
146 In each plot, we counted stems greater than 6 cm in diameter and calculated stem densities of
147 1900 stems ha^{-1} and 1100 stems ha^{-1} at the Upper Site and 1500 stems ha^{-1} and 900 stems ha^{-1} at
148 the Lower Site.

149 To reconstruct living biomass (hereafter referred to as biomass), two increment cores
150 (180˚ from one another) were collected from a haphazard subsample of approximately 50 trees
151 greater than 6 cm diameter at breast height (1.4 m above the ground; DBH; Supplemental Figure
152 1) within each plot (Babst et al. 2014b). A total of 201 trees were sampled across the four plots
153 (100 trees at Lower Site; 101 trees at Upper Site; Table S1). Increment cores were mounted,
154 sanded, and analyzed using established dendrochronology techniques (Stokes and Smiley 1967;
155 Speer 2010). We used a combination of skeleton plotting (Douglass 1941; Stokes and Smiley
156 1967) and the list method (Yamaguchi 2011) to crossdate (i.e. assign precise dates to individual
157 tree rings). Ring-width increments were then measured to the nearest 0.001mm and the
158 assigned dates were validated using the program COFECHA (Holmes 1983; Grissino-Mayer 2001).

159 The oldest sampled trees at all four plots were less than 100 years old (Table S2). At the
160 Upper Site, 76% of the trees were successfully crossdated (Table S1), resulting in a chronology
161 composed of 77 trees with an interseries correlation of 0.708 and an EPS of 0.961 (Table S2). Less
162 than 3% of the trees at the Upper Site were not considered effectively dated, either visually or
163 statistically, and 21% of the samples were unable to be analyzed due to complications during
164 sample extraction (Table S1). Cores from the upper site were often rotten, preventing a full

dendrochronological analysis. Of the trees collected at the Lower Site, 86% were crossdated, leaving 11% that did not effectively crossdate, and only 3% unable to be analyzed (Table S1). The chronology from this Lower Site was composed of 86 crossdated trees with an interseries correlation of 0.755 and an EPS of 0.975 (Table S2).

We found signs of fire or insect damage at the time of sampling (i.e. large amounts of coarse woody debris) and detected no significant growth release events in the period 1980-2011 (Supplemental Figure 2) or in records of management practices (Touchan et al. 1996; Anschueta and Merlan 2007; Allen et al. 2008). Low intensity fire events precipitously decreased after 1900 in this area and no evidence of a large fire event was present at the time of sampling at either site (Touchan et al. 1996; Allen et al. 2008). However, as with other proxy-based reconstructions, the 'fading record' can increasingly affect the accuracy of our biomass estimates back in time, as trees that were historically present at the sites may not have been present at the time of sampling and therefore could not be sampled (Swetnam et al. 1999; Babst et al. 2014a; Nehrbass-Ahles et al. 2014). We have taken two measures to account for this: 1) we have truncated the biomass reconstruction and analysis period at 1980, as this is the period of relatively little disturbance at these sites, and 2) we use reported broad-scale mortality rates for a comparable region in the western United States (van Mantgem et al. 2009; see *Mortality Uncertainty* section below).

DBH reconstruction and Gap Filling Techniques

For each individual tree, annual DBH was reconstructed by subtracting ring-width increments from the DBH measured in the field in June 2011 (Davis et al. 2009; Dye et al. 2016)

and then truncated at 1980 for analysis. Eccentricity in growth increment around the bole can be a confounding factor in DBH reconstructions, but a proportional method (Bakker 2005) resulted in minimal differences between the two techniques for our study period (r^2 = 0.99, Supplemental Figure 3). Minimal shrinkage due to drying is likely to occur, but was assumed negligible for this study (Cole 1977). For the DBH reconstruction, individual cores from the same tree were averaged. Cores that did not statistically crossdate were still used to estimate biomass after being visually checked for dating accuracy. These cores were not used to develop the tree-ring chronologies but were included in the mean biomass estimates. To reduce the potential size bias in the biomass estimate due to the high percentage of missing trees (25 trees at the Upper Site; 13 trees at the Lower Site; Table S1; Supplemental Figure 4), we gap filled the missing cores for which we have DBH measurements, but no ring widths using a generalized additive mixed model and the R package *mgcv* (Yee and Mitchell 1991; Wood 2004; Wood 2011). This model fit ring width (RW) as a function of fixed, interactive effects of species (SPECIES) and DBH at time of sampling (DBH) plus an additive a cubic smoothing spline through time for tree: $s(YEAR_{tree})$ (Eq. 1). Nested random effects of site, plot, and were also included. Gapfilling and all data analyses were performed using the R programming language (v. 3.2.1, R Core Team 2015).

[**Equation 1**] $$RW_{YEAR,TREE} = s(YEAR_{TREE}) + SPECIES \times DBH$$

Allometric uncertainty

Tree-level DBH reconstructions are transformed into biomass quantities through the use of allometric equations. As is common for most forests, no site-specific equations existed for most of our species, so we relied upon the allometric equations curated by Jenkins et al. (2004)

and Chojnacky et al. (2013) for total aboveground biomass allometric equations (Component 2; Jenkins et al. 2004). Our aim was to produce biomass estimates that reflect the upper limit of uncertainty possible, and we acknowledge that using site and species-specific equations based on expert opinion may produce more accurate and precise biomass estimates. We used all available equations meeting the component and species criteria of our sample (Table S3). Species-level equations were used for PSME, POTR, and PIPO. There are not any aboveground biomass equations listed for *Pinus ponderosa* in the Jenkins database. Therefore, we used A species-level PIPO equation was produced from a reanalysis of the Jenkins et al. (2004) database (Chojnacky *et al.* 2013). Genus-level *Picea* equations from Jenkins (2004) were used for PIEN because to total aboveground biomass equations were available. References for all equations used can be found in Supplemental Table 3.

We calculated allometric uncertainty using the 'allometry' package within the Predictive Ecosystem Analyzer (PEcAn, LeBauer et al. 2013, www.pecanproject.org). This package uses a Bayesian framework to combine multiple allometric relationships from Jenkins *et al.* (2004) into a single equation with corresponding parameter uncertainties. Using the PEcAn module, we simulated a distribution of 10,000 allometric equations for each taxa, preserving covariance among parameters and sampled from the last 5,000 equations to allow for Markov chain Monte Carlo (MCMC) convergence. We randomly pulled 500 equations for each tree from the distribution for each species and used those to calculate tree-level biomass. To preserve the allometric uncertainty at the tree level while scaling up to the site level, we averaged across all individuals at the site, randomly selecting a single biomass estimate for each tree. This resulted

232 in 500 estimates of biomass for each site. Allometric uncertainty was then described as the 95%
233 confidence interval around the mean-centered distribution of cumulative biomass estimates.
234
235 *Subsampling Uncertainty*
236 Because tree rings and biomass estimates came from a subsample of 50 trees from each
237 plot, our biomass calculations used the mean tree growth at the site level to characterize changes
238 in biomass through time at the stand level. This allowed us to not only present a mean estimate
239 for biomass change, but also quantify the uncertainty present in forest-level biomass
240 accumulation arising through the variability in individual tree growth. This approach relies on the
241 assumption that our haphazard sample of 50 trees accurately represents the size and species
242 distribution of all individuals in the plot. To calculate the subsampling uncertainty, we first
243 calculated annual biomass increment for each tree using a first-difference approach and mean-
244 centered the increment distribution. We describe the subsampling uncertainty using the 95%
245 confidence interval around this observed distribution of values. We used both dated and gap-
246 filled trees for this calculation, as it protects against a potential size bias of using only dated trees
247 (Supplemental Figure 4).
248
249 *Sampling Uncertainty*
250 Sampling multiple locations in a site is the most common method of providing uncertainty
251 in field-based biomass estimates. This uncertainty arises from spatial heterogeneity resulting in
252 variable densities among plots. We characterized this location-based sampling uncertainty in
253 forest density as the mean biomass for a tree at each site (kg per tree; averaged across both
254 plots) times the density for each plot (trees per m^2). To robustly characterize sampling

255 uncertainty, ideally all individuals in a plot would be sampled, summed to the plot level, and then
256 that total could be averaged across more than two plots, but this was not possible in our study.
257 Thus, we describe the uncertainty in biomass estimates from sampling uncertainty in our study as
258 the range based on the densities observed in our two plots.
259
260 *Mortality Uncertainty*
261 Long-term census data were not available for our study sites and therefore we have no
262 records of how the loss of individuals to mortality affects biomass reconstructions at our site.
263 Therefore, to account for the mortality-based biomass losses through time, we used regional
264 mortality estimates from van Mantgem *et al*. (2009) to simulate background mortality processes
265 and adjust the stand density applied to per-tree biomass estimates through time. van Mantgem
266 et al. (2009) reported a baseline mortality rate in 1979 of 0.4843 ± 0.0941% yr^{-1} (mean ± SE) with
267 an annual increase in that rate of 0.024 ± 0.027% yr^{-1}. We calculated mortality uncertainty in our
268 biomass estimates by using these reported values and error estimates to generate a distribution
269 of modifications to our initial stem densities in time. To do this, we assumed the values
270 presented by van Mantgem *et al.* were normally distributed and converted standard error to
271 standard deviation using the reported *n*=9. We simulated a normal distribution of baseline
272 mortality rates for 1979 that then compounded and increased in time to the present. Thus, the
273 mortality rate in year *t* starting in 1980 can be described as the percent mortality rate (Mortality)
274 in the previous year with in 1979 (normal, μ=0.4843, σ =0.2823) plus a fractional increase in that
275 mortality rate (Eq. 2, van Mantgem 2009). The annual increase in mortality rate is described as a
276 normal distribution (*normal*, μ = 0.024, σ = 0.081) times the previous year's mortality rate.

Density in each year can then be simulated from the present into the past as a function of the initial density in time (t+1) plus the percentage of stems lost to mortality in that year (Eq. 3).

Equation 2: $Mortaltiy_t = Mortaltiy_{t-1} + Mortaltiy_{t-1} \times Increase$

Equation 3: $Density_t = Density_{t+1} + Density_{t+1} \times Mortiality_t$

Using the errors reported by van Mantgem *et al.* (2009), we simulated 500 possible mortality-adjusted year-specific densities that were then multiplied with per-tree estimates of biomass. Negative simulated values that would represent recruitment were discarded in this process so that mortality would increase biomass estimates. Mortality uncertainty is described as the 95% confidence interval in the difference between biomass estimates using mortality-adjusted density relative to a static plot density using the stem density values observed in 2011.

Total Uncertainty Calculation

For both the cumulative and the interannual biomass reconstructions, the total uncertainty was calculated by first calculating the deviation of the upper and lower 95% confidence interval bound from the mean baseline biomass estimate: mean tree biomass estimate times mean plot density for each area of uncertainty. The upper and lower bounds for each area were then added in quadrature to quantify the total uncertainty in field-based biomass estimates. The percent contribution of each component was calculated as the component divided by the sum of all sources of uncertainty.

299 *Climate Response Analyses*

300 We assessed the response of tree growth and above ground biomass increment to
301 interannual variability in precipitation and temperature through a series of Pearson correlation
302 analyses. We compared the growth-climate relationships of four tree-ring width chronologies to
303 that of the mean annual biomass increment (BM) time series per site. Three tree-ring
304 chronologies were calculated per site from our samples using 1) all crossdated trees, 2) the
305 largest 10% of crossdated trees, and 3) the smallest 10% of crossdated trees (hereafter referred
306 to as All, Large, and Small, respectively). At the Upper and Lower Sites, respectively, the All
307 chronologies represent diameter ranges of 6.8 – 53.6 cm and 10.2 – 40.5 cm, the Small
308 chronologies are composed of diameters ranging from 6.8 – 10.0 cm (n = 11) at the Upper Site
309 and 10.2 – 13.1 cm (n = 10) at the Lower Site. The Large chronologies are composed of diameters
310 from 34.8 – 53.6 cm (n = 11) at the Upper Site and 34.5 – 40.5 cm (n = 10) at the Lower Site. We
311 obtained additional tree-ring width chronologies that were specifically sampled for
312 dendroclimatic purposes ('ITRDB') at Valles Caldera from the International Tree-Ring Data Bank
313 that were built from similar species at similar elevations. We used the chronology developed by
314 Touchan et al. (PSME; 2011) and Brice et al. (PIPO; 2013) to evaluate the growth-climate
315 responses at the Upper Site and Lower Site, respectively. Each chronology was generated using a
316 30-yr cubic smoothing spline to detrend individual series and the biweight robust mean was
317 calculated to create a site level chronology (Cook 1985; Cook and Peters 1997). The BM time
318 series was not detrended, because detrended data would not be used in land-surface model data
319 assimilation, and detrending had little effect on the overall growth-climate response
320 (Supplemental Figure 5). We compared the BM time series and tree-ring width chronologies to

PRISM temperature and precipitation data (PRISM Climate Group 2004). We extracted climate data for each of our sampled sites and aggregated to the following seasons: previous fall (pFall) = pSept, pOct, PNov; Winter = pDec, Jan, Feb; Spring = Mar, Apr, May; Summer = June, July, Aug). We then used a Pearson's correlation analysis on the common overlapping period of all time series (1980-2007) to determine significant climate correlations with statistical significance defined as $p < 0.05$.

To determine how the full range of uncertainties might affect the biomass growth-climate relationship, we bootstrapped 30,000 independent, random draws with replacement from the observed distribution of each area of uncertainty: allometry, sub-sampling, sampling, and mortality. 500 values from each source of uncertainty were independently drawn and added together in quadrature to generate 30,000 simulated BM time series. We then performed a similar correlation analysis as described above to assess the uncertainty in growth-climate relationships of the series. We assessed the differences in climate response from the biomass increment responses of 1) all trees, 2) the largest 10% of trees, 3) the smallest 10% of trees at each site. The size categories were based off the same DBH ranges as stated above for the tree-ring width chronologies. We identified relationships as significant if the 95% CI of the critical values did not encompass zero.

Results

The relative contribution of sources of uncertainty differed between cumulative biomass estimates and interannual biomass estimates. The mean cumulative biomass at the time of sampling at the Lower Site (PIPO) was 20.95 kg m^{-2}, with a lower 95% CI of 18.54 kg m^{-2} and an upper 95% CI of 23.54 kg m^{-2}, and the mean biomass of the Upper Site (PSME/PIEN) was 24.47 kg

344 m^{-2}, with a lower 95% CI of 16.96 kg m^{-2} and an upper 95% CI of 35.19 kg m^{-2} (Figure 1). With the
345 exception of the allometric uncertainty, the ranges of uncertainty are comparable across both
346 sites (Table S1). At the Upper Site, allometric and mortality components account for over 75% of
347 the total uncertainty in cumulative biomass, with uncertainty in the allometric equations
348 accounting for 58 ± 9% (mean ± SD; 1980-2011) and mortality accounting for 24 ± 11% from
349 1980-2011 (Figure 2; Table S1). At the Lower Site, allometric uncertainty accounts for 34 ± 11%
350 and mortality accounts for 42 ± 16% of the total uncertainty in cumulative biomass. The
351 subsampling uncertainty contributed the least to the overall cumulative biomass uncertainty at
352 the upper and Lower Sites (7 ± 2% and 8 ± 3%, respectively; Figure 2; Table S1).

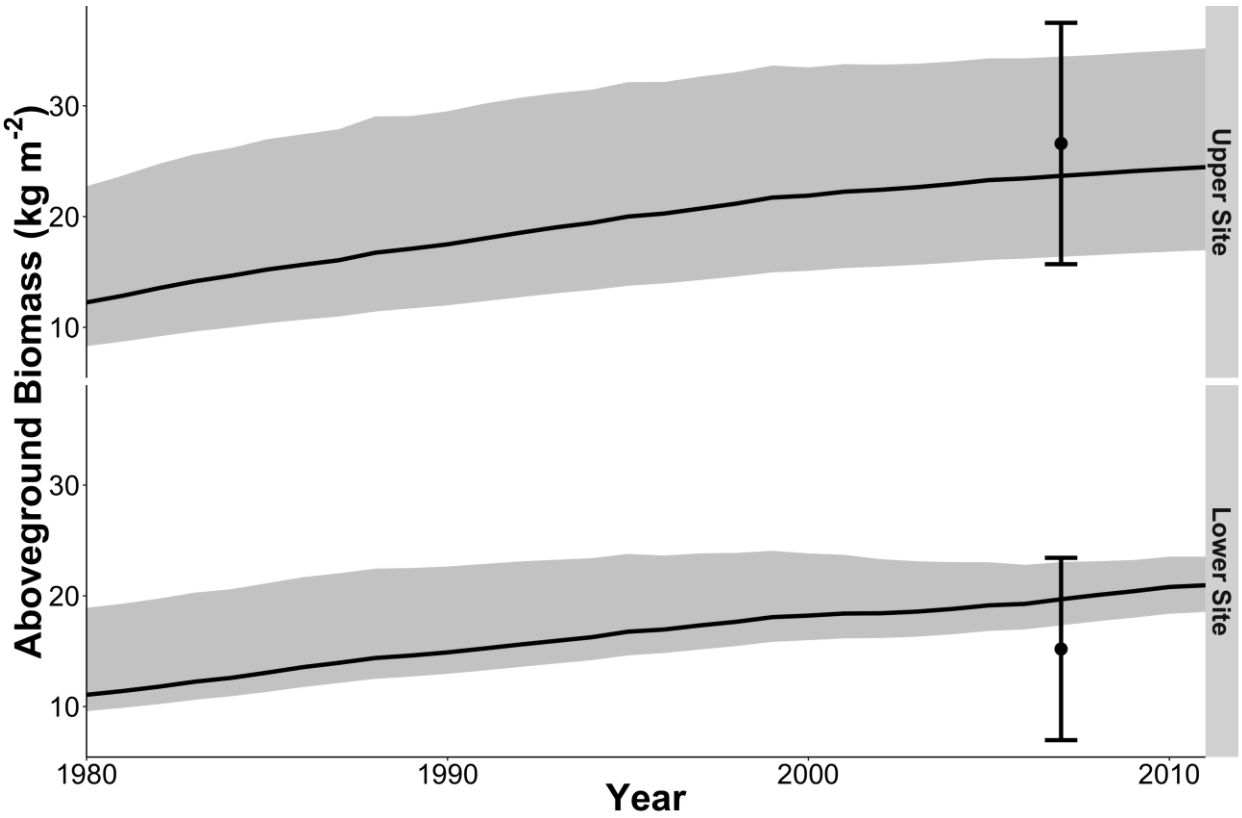

Figure 1. Site-level cumulative biomass estimates with total uncertainty ranges for an upper elevation Engelmann spruce dominated (Upper Site) and lower elevation ponderosa pine dominated forest (Lower Site) at the Valles Caldera, NM. The dark black line represents the mean cumulative biomass estimate traditionally reported, and the shaded grey area is the 95% CI of biomass from adding all sources of uncertainty together in quadrature. Points and error bars represent an independent assessment (Mean ± 1.96*SD; n = 4) of living biomass (assuming a 50% carbon content) from 2007 for both sites (Anderson-Teixeira et al. 2011 Table S2).

353

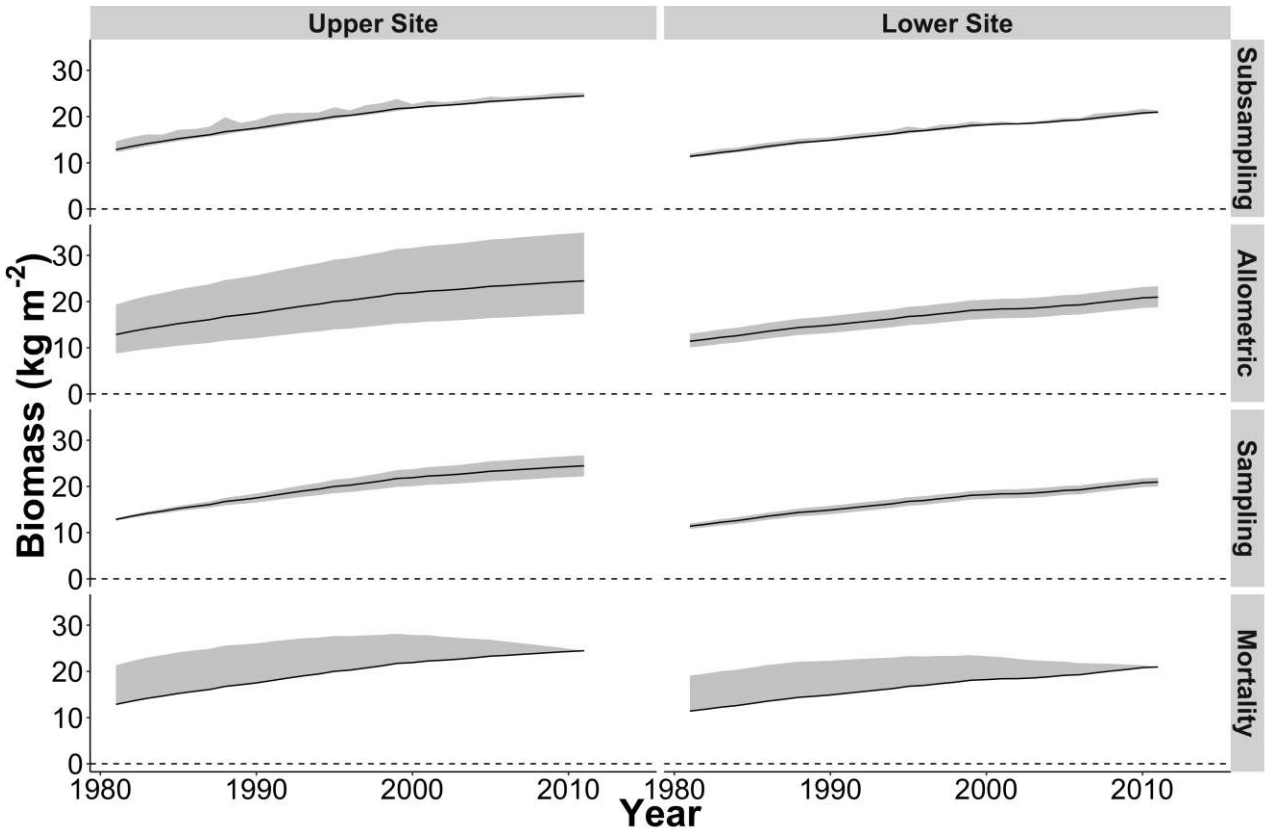

Figure 2. Cumulative tree-ring derived biomass estimates for the Upper Site (left column) and the Lower Site (right column) at the Valles Caldera. The black line represents the biomass calculated for the mean allometric equation for each site, and the shaded area is the 95% confidence interval for each source of uncertainty.

The mean interannual biomass increment at the Upper Site was 0.39 ± 0.16 kg BM m^{-2} yr^{-1} with an upper 95% CI of 1.88 ± 0.76 kg BM m^{-2} yr^{-1} and a lower 95% CI of -0.08 ± 0.08 kg BM m^{-2} yr^{-1}. The negative lower CI indicates the potential impact that the mortality uncertainty has on the overall biomass uncertainty from year to year. At the Lower Site the mean annual biomass increment was 0.32 ± 0.3 kg BM m^{-2} yr^{-1} with an upper 95% CI of 1.02 BM m^{-2} yr^{-1} and a lower 95% CI of -0.04 kg BM m^{-2} yr^{-1}. Subsampling uncertainty accounted on average for more than 70% of the interannual biomass subsampling uncertainty at both the Upper and the Lower Sites (70 ± 10% and 71 ± 14%, respectively; Figure 3; Table S1). Second to subsampling uncertainty, mortality uncertainty accounted for 21 ± 16% of the total annual biomass subsampling

364 uncertainty at the Lower Site and 16 ± 13% at the Upper Site (Figure 3; Table S1). At the Lower
365 Site, sampling uncertainty contributed the least to the overall subsampling uncertainty (3 ± 2%),
366 whereas allometric uncertainty composed 4 ± 1% (Figure 3). Allometric uncertainty played a
367 larger role at the Upper Site, contributing 8 ± 2%, and sampling uncertainty contributed the least
368 with 5 ± 2% of the overall subsampling uncertainty.
369

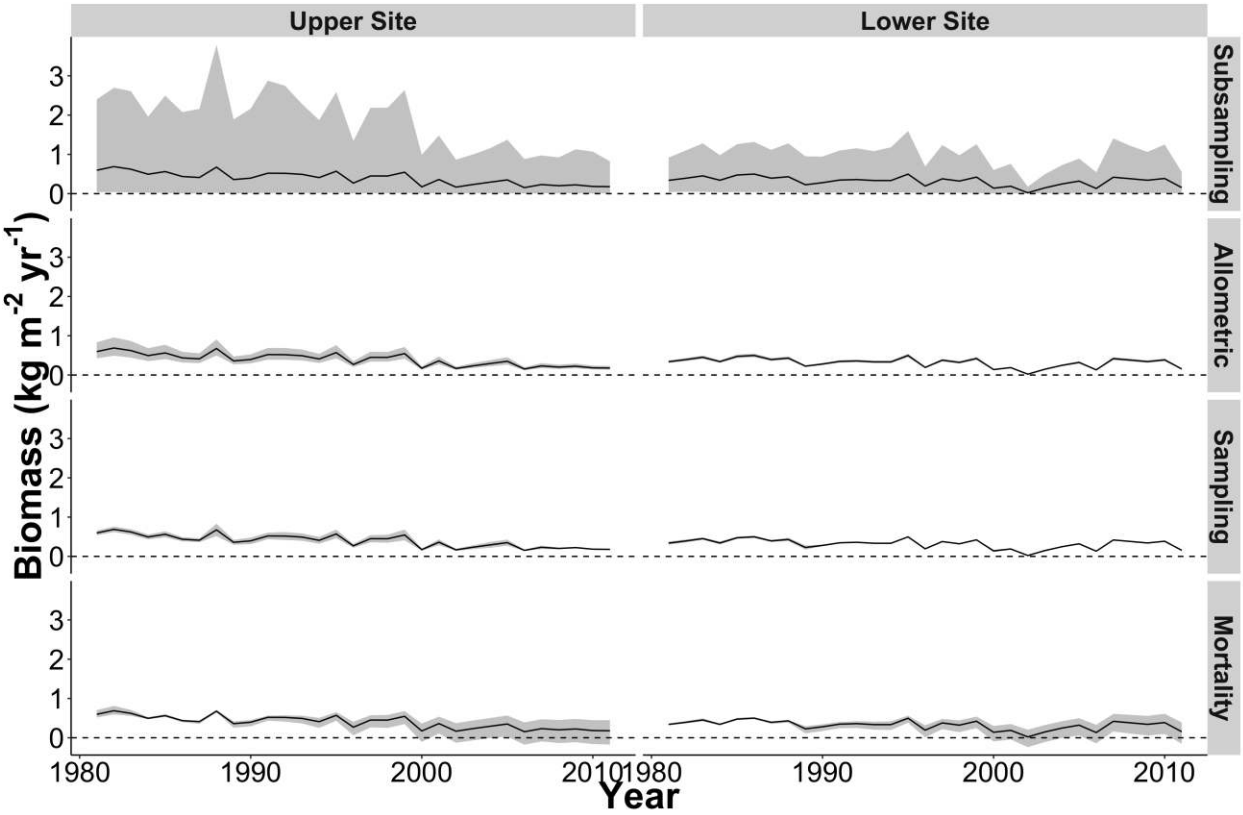

Figure 3. Interannual tree-ring derived biomass estimates for the Upper Site (left column) and the Lower Site (right column) at the Valles Caldera. The black line represents the mean interannual biomass increment calculated for each site, and the shaded area is the 95% confidence interval for each source of uncertainty.

The climate sensitivities of the BM time series at both sites were similar to that expressed by the four tree-ring width time series (Figure 4). A signal typical of the Southwestern US can be seen at both sites and across all chronologies analyzed, with negative relationships with spring and summer temperatures and positive relationships with previous fall, winter, and spring precipitation (Figure 4). At the Upper Site, the BM time series generally reflected the signal in the All chronology and the ITRDB chronology. However, the BM time series showed a significant negative correlation with summer temperature and a significant positive correlation with summer precipitation, when neither the All chronology nor the ITRDB chronology do so (Figure 4). The Large chronology at the Upper Site showed similar summer correlations to those of the

BM time series, indicating that in the summer months the largest trees at the Upper Site are contributing more to this particular climate response (Figure 4). The growth responses are relatively consistent between the Large chronology and the Small chronology, with notable differences in both the summer temperature and precipitation responses. In both cases, the growth response of the Large chronology was stronger than that of the Small chronology. At the Lower Site, the BM time series showed a significant negative relationship with temperature during the previous fall and the current summer, but not a significant relationship with spring temperatures. This is different than any of the tree-ring chronologies from this site, which all show a significant negative response to spring temperature (Figure 4).

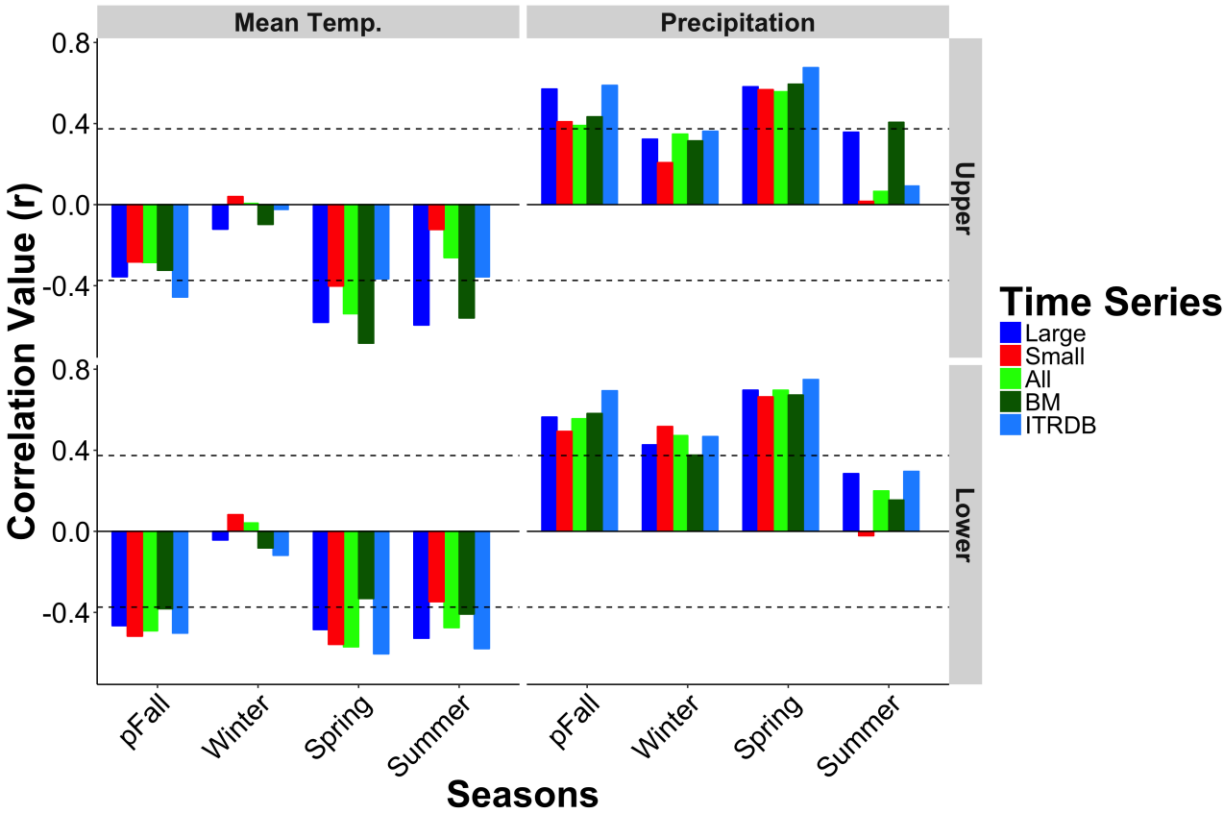

Figure 4. Seasonal (previous Fall, Winter, Spring, Summer) growth-climate response of mean biomass increment estimates (dark green) and four tree-ring chronologies (Large, Small, All, ITRDB) with mean temperature and total precipitation at an upper (Upper Site) and a lower (Lower Site) elevation site in the Valles Caldera, NM. The Large chronology (blue) is composed of the largest 10% of trees by DBH and the Small chronology (red) is composed of the smallest 10%. The ITRDB chronology (light blue) was gathered from ITRDB (Upper Site: Touchan et al. 2011; Lower Site: Brice et al. 2013). The mean biomass increment time series (light green) represents the mean annual biomass increment for each site. Significant responses were identified as those values exceeding the ($\alpha = 0.05$) significance criterion (dashed line).

The general growth-climate relationships for the biomass increment time series using the full uncertainty distribution were similar to those for the mean BM and tree-ring chronology assessment, but illustrate the breadth of climate response upon translating tree-ring data into biomass (Figure 4 and Figure 5). Across both sites, the smallest trees show a relatively narrow range of climate responses, compared to the largest trees (Figure 5). Once transformed into biomass, the mean summer growth response of the Small trees is strengthened, whereas the

mean response of the largest trees appears to be muted, likely due to the highly-varied climate response (Figs. 4 and 5).

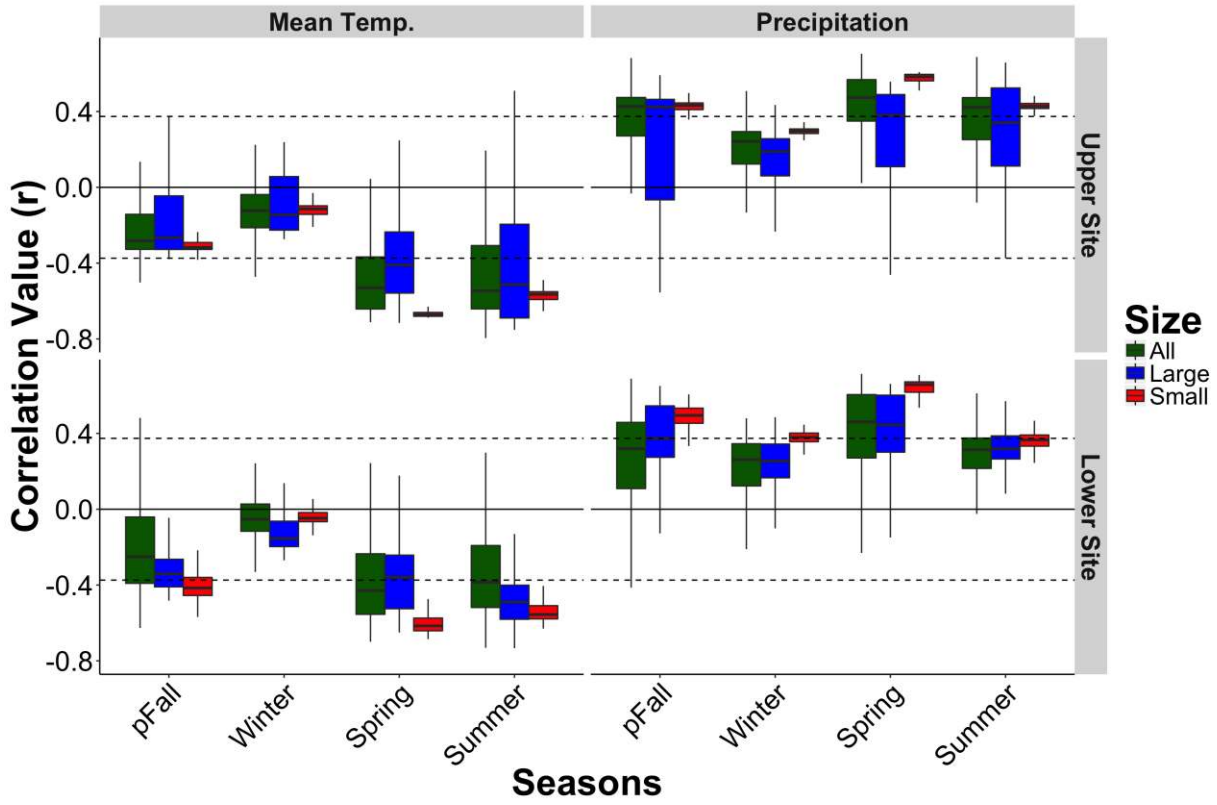

Figure 5. Distributions of growth-climate relationships for simulated biomass time series from an upper elevation (Upper Site; PIEN) and a lower elevation (Lower Site; PIPO) forest in the Valles Caldera, NM. The Large time series is based on the largest 10% of trees, the Small time series is based on the smallest 10% of trees, and the All time series is composed of all trees sampled. Distributions were generated by bootstrapping, with replacement, 30,000 time series meeting each of the three criteria and performing a Pearson's correlation analysis. Solid bars refer to the mean r-value.

Table 1. Mean ± SD for cumulative and incremental living aboveground biomass uncertainty ranges (kg m^{-2}) for 1980 – 2011 of major sources of variability at an upper elevation and a lower elevation forest in the Valles Caldera, NM. Total uncertainty is calculated by adding the upper and lower 95% confidence intervals of each area of uncertainty in quadrature.

Source	Cumulative Range (kg BM m^{-2})		Incremental Range (kg BM $m^{-2}y^{-1}$)	
	Upper Site	Lower Site	Upper Site	Lower Site
Allometric	14.88 ± 2.14	3.89 ± 0.47	0.20 ± 0.09	0.15 ± 0.06
Subsampling	1.84 ± 0.76	0.98 ± 0.30	1.84 ± 0.76	3.19 ± 1.25
Sampling	2.86 ± 1.35	1.78 ± 0.21	0.13 ± 0.07	0.85 ± 0.36
Mortality	6.39 ± 2.82	5.39 ± 2.50	0.30 ± 0.19	0.61 ± 0.40
Total	17.67 ± 0.93	8.15 ± 1.73	1.95 ± 0.70	1.06 ± 0.25

Discussion

The application of tree rings to aboveground biomass assessments provides time series of biomass change that are similar to, but more finely-resolved than estimates from periodic census data (Dye et al. 2016). However, appropriate uncertainties must be reported alongside these estimates to facilitate comparisons among disparate locations and data types. Without the accompanying uncertainties, comparisons between similar forest types can be misleading. For example, our mean estimate of total aboveground biomass at the Lower (PIPO) site was 19.7 kg BM m^{-2} in 2007. Without uncertainties or margins of error, this would appear high when compared to comparable values from similar regions and forest types. A study whose sites are proximal to our own estimated aboveground biomass at the Lower (PIPO) site to be 15.3 ± 4.2 kg BM m^{-2} (mean ± SD; Anderson-Teixeira 2011 Table S2) in 2007. In other southwest PIPO forests, Kaye et al. (2005) estimated aboveground biomass has been estimated as 12.7 ± 2.2 kg BM m^{-2} in

419 1995, and Finkral et al. (2008) observed a range of biomass of 5.9—14.1 ± 3.0 kg BM m^{-2}.
420 However, when the full range of uncertainty is considered, our aboveground biomass estimate
421 (17.3—23.0 kg BM m^{-2}; 95% CI) is consistent with these previously reported values.
422 We found that uncertainty due to the choice in the allometric equation is the largest
423 contributor to the overall uncertainty in cumulative biomass estimates at our site (Figure 2).
424 Choice of allometric equation has substantial influence over the initial value of biomass
425 reconstructions (Chave et al. 2004), however, this area of uncertainty is seldom reported, despite
426 both the plethora and dearth of equations that can exist for any one species (Jenkins et al. 2004,
427 Chojnacky et al. 2013, Supplemental Table 3). The most commonly reported uncertainty
428 associated with biomass quantities is the variability among plots, what we term 'sampling'
429 uncertainty. The spatial heterogeneity of biomass across the landscape can be quite large, with
430 the 95% CI consisting of between 34% and 100% of the mean biomass estimates reported by
431 other studies in similar forest types (Kaye et al. 2005, Finkral et al. 2008, Anderson-Teixeira et al.
432 2011). The uncertainties that accompany tree-ring derived estimates of aboveground biomass are
433 also influenced by a combination of temporally static factors such as allometric equation choice,
434 and temporally dynamic factors such as annual increment and mortality rate. Yet, despite the
435 process involved in transforming tree-ring increments into estimates of aboveground biomass,
436 the growth-climate relationships observed in our tree-ring chronologies persist (Figures 4 and
437 Figure5). This means that, at least in climate-sensitive regions such as the semi-arid, American
438 Southwest (St. George and Ault 2014), the observed growth-climate relationships will be
439 accurately represented in the aboveground biomass estimates that are subsequently
440 incorporated into large-scale modeling frameworks.

441 Not all trees in the stand respond similarly to interannual variation in climate.
442 Subsampling uncertainty accounts for at least 70% of the total interannual biomass increment
443 uncertainty, and arises when extrapolating the observed, individual-level growth patterns to
444 represent that of the entire stand. However, the represented climate signal may change
445 depending on the climate sensitivity of the species sampled and the manner in which those trees
446 are selected (Nehrbass-Ahles et al. 2014; St. George and Ault 2014). The crossdating process is
447 integral to the proper quantification of this area of uncertainty to temporally align the annual
448 growth of individual trees (Black et al. 2016). The mean growth increment is often used in
449 dendrochronology to characterize and understand the mechanisms that affect tree growth at the
450 site level. However, using the mean value in these analyses can overlook factors that influence
451 tree growth, such as stand dynamics or size. For example, Nehrbass-Ahles et al. (2014) found
452 that sampling design had little influence on the climate signal that was expressed by the standard
453 mean tree-ring chronology, as using the mean has a stabilizing effect on the expressed climate
454 signal. We found a similar result (Figure 4): the growth-climate responses of the mean tree-ring
455 width chronologies and BM time series are similar. However, we see differing strengths in the
456 correlations with climate of Large and Small trees (Figure 4; Figure 5), which may indicate how
457 asymmetric competition within the stand influences climate responses (Canham et al. 1994;
458 Rollinson et al. 2016). The mean forest response characterizes the general growth-climate
459 relationship of the larger, more dominant trees (Figure 3; Figure 4), and by presenting the
460 subsampling uncertainty alongside the mean biomass estimate we can gain a more nuanced view
461 of the growth-climate relationships of non-dominant forest components (Rollinson et al. 2016).
462 Tree-ring increments cannot provide a time series of interannual changes in bark thickness. For

463 our calculations we have assumed a constant bark thickness with a changing ring-width
464 increment, and recognize that this may not be an accurate depiction of allocation of resources to
465 bark through time. The subsampling uncertainty is present at both the cumulative and
466 incremental time steps, but is a relatively minor component compared to other sources of
467 uncertainty at the cumulative level (Figure 2).

468 The choice of allometric equation strongly influences the cumulative biomass estimate
469 (Figure 2), but had a minimal effect on the interannual biomass increment (Figure 3). At the
470 Upper Site, allometric uncertainty comprised 57 ± 8% of the total uncertainty around cumulative
471 biomass, whereas at the Lower Site it only contributed 34 ± 11% to the overall cumulative
472 uncertainty. Chave et al. (2004) found that allometric uncertainty in tropical trees can dominate
473 over sampling uncertainty. We also see that allometric uncertainty dominates the cumulative
474 biomass uncertainty at our sites. However, at the incremental scale, its influence is less than that
475 of the subsampling variability (Figure 2 and Figure 3). Allometric equations allow for diameter
476 reconstructions to be transformed into biomass estimates, but uncertainties exist within and
477 among allometric equations (Chave et al. 2004; Nickless et al. 2011; Babst et al. 2014a). Large
478 syntheses and databases (Jenkins et al. 2004; Chojnacky et al. 2013) have made allometric
479 equations more accessible, but the variability in equations among species, size classes, and across
480 sites (Ketterings et al. 2001) make it difficult to identify the most appropriate equation for a given
481 study.

482 Ideally, any reconstruction of biomass would rely on site-specific allometric equations, but
483 even site-specific equations will contain parameter uncertainties that should be reported to
484 facilitate easier comparisons between sites and among equations. By using a Bayesian approach

485 (LeBauer et al. 2013) we generated parameter-based uncertainties that included all of the
486 equations available for each species from the Jenkins et al (2004) database, and thus have
487 illustrated the full range of biomass estimates possible from these equations. Using all available
488 equations has likely increased the uncertainty in our biomass estimates. However, due to strong
489 influences of fine-scale environmental variability and phenotypic plasticity in growth form
490 (Weiner 2004), even locally-derived equations may not accurately represent all trees sampled in
491 any one study (Chave et al. 2004).

492 Sampling uncertainty is influenced by the forest structure and the chosen sampling
493 design. A sampling design that both accurately represents the variability among individuals
494 within the forest, yet is feasible to implement, has always been a concern in ecological research
495 (Botkin and Simpson 1990; Pacala et al. 1996; Mackenzie and Royle 2005). Nehrbass-Ahles et al
496 (2014) recently advocated for the use of 25m fixed radius plots as a practical means to estimate
497 aboveground biomass in European forests. However, in our least dense plot (0.09 trees m^{-2}) this
498 would have resulted in 176 trees per plot, whereas a mean of 57 trees were present in the
499 Nehrbass-Ahles et al. (2014) plots. The range of sampling uncertainties at the Upper and Lower
500 sites was comparable to those reported for nearby sites within the Valles Caldera. In 2007, the
501 living biomass at the site was reported as 26.6 ± 10.8 kg BM m^{-2} (mean ± 95% CI; assuming a 50%
502 C content; Anderson-Teixeira et al. 2011 Table S2) and 15.2 ± 8.2 kg BM m^{-2} at the Upper and
503 Lower sites, respectively (Figure 1). The reported uncertainty overlaps with the full range of
504 uncertainty observed at our sites (Figure 1), but is larger than the range of our reported sampling
505 uncertainty (1.35 and 0.21 kg BM m^{-2} at the Upper and Lower Sites, respectively; Anderson-
506 Teixeira 2011 Table S2). It is likely that the previous study analyzed a dataset with greater spatial

507 diversity, but the reported uncertainties facilitate comparisons between the two biomass
508 estimates.

509 Tree-ring investigations of mortality are traditionally focused on establishing the timing of
510 an event (Foster 1988; Swetnam and Lynch 1989; Daniels et al. 1997), but quantifying the extent
511 of a past mortality events is highly situational (Rubino and McCarthy 2004). Our sites were
512 relatively even-aged and no major anthropogenic or natural disturbances were recorded over the
513 lifespan of most trees (Touchan et al. 1996; Anschueta and Merlan 2007; Allen et al. 2008;
514 Supplemental Figure 2), but we have limited our analysis to the period 1980-2011 to overcome
515 the challenges associated determining a representative mortality rate. Long-term census data
516 have been used to determine timing of individual mortality events, but these datasets are sparse
517 and time consuming to generate (Eisen and Plotkin 2015). However, when these data are
518 available, tree-ring estimates of aboveground biomass at the same site fall within the 95%
519 confidence interval of the permanent plots, suggesting that, to a point, tree rings can be used to
520 accurately depict aboveground carbon dynamics (Dye et al. 2016). We chose to use generalized
521 mortality values from the interior western US (van Mantgem et al. 2009) to estimate changing
522 stand densities and thus biomass load back through time, but localized mortality rates or detrital
523 biomass loads would increase the accuracy of this source of uncertainty. We acknowledge that
524 mortality is more episodic than is indicated by our continuous mortality rate, and often occurs as
525 sudden die-off events (Allen et al. 2010) or gap dynamics (Pederson et al. 2014) rather than a
526 constant self-thinning rate that we describe in this paper. These die-off events would manifest
527 themselves in the existing tree-ring record as synchronous increases in the growth (release
528 events) of nearby surviving trees, and thereby affecting the mortality uncertainty of the biomass

529 reconstruction (Lorimer and Frelich 1989). There is no evidence that such an event occurred at
530 the sites we studied from 1980 through 2011 (Supplemental Figure 2). Mortality is a difficult
531 process to constrain, both in the lab (Fisher et al. 2010) and in the field (Allen et al. 2010), but
532 continued measurement efforts across diverse sites will greatly improve the accuracy of mortality
533 estimates from isolated stands to landscape-level processes.
534 The climate response patterns in both our chronologies and biomass estimates adhere to
535 what is known about forests in this region: they are strongly influenced by winter precipitation
536 and spring temperatures, prior to the hot pre-monsoon summer conditions (St George et al.
537 2010; Touchan et al. 2011; Griffin et al. 2013; St George and Ault 2014). In general, growth-
538 climate relationships of the BM time series are similar to that of the mean tree-ring chronology
539 based on all trees, with the exception of the increased summer precipitation response (Figure 4).
540 Detrending the biomass data did little to change the growth-climate relationship (Supplemental
541 Figure 5). The effect of the large contribution of the incremental upscaling uncertainty (Figure 3)
542 can be seen in the different climate responses of large and small trees (Figure 4). Using only the
543 growth-climate response of the largest trees does change the observed pattern at both sites
544 (Figure 3 and Figure 4). On a per-stem basis, large trees disproportionately contribute more to
545 the total forest biomass estimate than smaller trees. Therefore, it is not unreasonable that the
546 growth signal of the largest trees most closely resemble the forest-level response (Lutz et al.
547 2012; Slik et al. 2013). The differences between responses of Large and Small trees could indicate
548 the impacts assymetric competition or access to water sources may have on climate respons
549 (Rollinson et al. 2016, Kerhoulas et al. 2013). Both forests had relatively simple canopy
550 structures, but the broad response of the Large trees suggests that they are still experiencing

551 varied environmental and ecological conditions that affects their sensitivity to climate (Carnwath
552 et al. 2012).

553 Accurately projecting future changes to the terrestrial carbon cycle depend in part on
554 characterizing the long term response of ecosystems to climate (Friedlingstein et al. 2006). To
555 this end, tree rings are useful in estimating aboveground biomass for various forest ecosystems
556 over longer time periods (Graumlich et al. 1989; Babst et al. 2014b; Babst et al. 2014a; Nehrbass-
557 Ahles et al. 2014; Dye et al. 2016), but we must continue to develop this technique to better
558 understand the terrestrial carbon cycle. Individual trees compose the forest and it is the growth
559 response of these individuals that affects the concerted ecosystem response. As tree rings are
560 increasingly used in studies of carbon dynamics (Babst et al. 2014a, Nehrbass-Ahles et al. 2014,
561 Dye et al. 2016), the methods must continue adapt to understand the growth-climate
562 relationships at multiple scales. In the case of terrestrial carbon and biomass studies, our study
563 suggests that both climate and ecological variables such as stand density and competition have
564 strong effects on tree growth and that the ecosystem response to climate can be more variable
565 than what is represented by a subsample trees in a particular age or size class. Tree rings provide
566 a means to generate both cumulative and interannual increment estimates of aboveground
567 biomass, but the lack of uncertainty estimates limits the inferences and comparisons that can be
568 made (Keenan et al. 2011). Uncertainty estimates will facilitate the creation of large-scale
569 biomass networks, providing an empirical basis from which to model carbon cycle dynamics.

Author Contributions

Alexander, Trouet, and Moore conceived of main analyses and conducted field sampling. Alexander performed tree ring analysis and data generation. Alexander and Rollinson contributed to code generation and uncertainty analyses. All authors contributed to intellectual project development and to manuscript preparation and writing.

Acknowledgements

This research was supported by the DOE Regional and Global Climate Modeling program DE-SC0016011 and by the University of Arizona Water, Environment, and Energy Solutions (WEES) and Sustainability of Semi-Arid Hydrology and Riparian Areas (SAHRA) programs. FB acknowledges funding from the Swiss National Science Foundation (grant #P300P2_154543) and the EU H2020 Program (grant 640176, "BACI"). The authors would like to thank Emily Dynes, Ian Schiach, and Bhaskar Mitra for help with sample collection, Amy Hudson for statistical input, and Marcy Litvak for her helpful comments and insights into the Valles Caldera.

Conflict of Interest Statement

The authors declare that they have no conflicts of interest.

Literature Cited

Ahlström A, Raupach MR, Schurgers G, et al (2015) The dominant role of semi-arid ecosystems in the trend and variability of the land CO2 sink. Science 348:895–899.

Allen CD, Anderson RS, Jass RB, Toney JL (2008) Paired charcoal and tree-ring records of high-frequency Holocene fire from two New Mexico bog sites. International Journal of Wildland Fire 17:115–130.

Allen CD, Macalady AK, Chenchouni H, et al (2010) A global overview of drought and heat-induced tree mortality reveals emerging climate change risks for forests. Forest Ecology and Management 259:660–684.

Anderson-Teixeira KJ, Delong JP, Fox AM, et al (2011) Differential responses of production and respiration to temperature and moisture drive the carbon balance across a climatic gradient in New Mexico. Global Change Biology 17:410–424.

Anschueta KF, Merlan T (2007) More than a scenic mountain landscape: Valles Caldera National Preserve land use history. Mountain Res. United State Department of Agriculture. Forest Service. Rocky Mountain Research Station., Fort Collins, CO

Babst F, Alexander MR, Szejner P, et al (2014a) A tree-ring perspective on the terrestrial carbon cycle. Oecologia 176:307–322.

Babst F, Bouriaud O, Alexander R, et al (2014b) Toward consistent measurements of carbon accumulation: A multi-site assessment of biomass and basal area increment across europe. 32:153–161.

Bakker JD (2005) A new, proportional method for reconstructing historical tree diameters. Can J For Res 35:2515–2520.

Belmecheri S, Babst F, Wahl ER, et al (2015) Multi-century evaluation of Sierra Nevada snowpack. Nature Climate Change 6:2–3.

Biondi F (1999) Comparing Tree-Ring Chronologies and Repeated Timber Inventories as Forest Monitoring Tools. Ecological Applications 9:216–227.

Black BA, Griffin D, van der Sleen P, et al (2016) The value of crossdating to retain high-frequency variability, climate signals, and extreme events in environmental proxies. Global Change … 22:2582–2595.

Bonan GB (2008) Forests and climate change: Forcings, feedbacks, and the climate benefits of forests. Science 320:1444–1449.

Botkin DB, Simpson LG (1990) Biomass of the North American Boreal Forest: A Step toward Accurate Global Measures. Biogeochemistry 9:161–174.

Brice B, Lorion KK, Griffin D, et al (2013) Signal Strength in Sub-Annual Tree-Ring Chronologies From Pinus Ponderosa in Northern New Mexico. Tree-Ring Research 69:81–86.

Canham CD, Finzi AC, Pacala SW, BURBANK DH (1994) Causes and Consequences of Resource

627 Heterogeneity in Forests - Interspecific Variation in Light Transmission by Canopy Trees. Can J For Res
628 24:337–349.

629 Carnwath GC, Peterson DW, Nelson CR (2012) Effect of crown class and habitat type on climate–growth
630 relationships of ponderosa pine and Douglas-fir. Forest Ecology and Management 285:44–52.

631 Chave J, Condit R, Aguilar S, et al (2004) Error propagation and scaling for tropical forest biomass
632 estimates. Philos Trans R Soc Lond, B, Biol Sci 359:409–420.

633 Chojnacky DC, Heath LS, Jenkins JC (2013) Updated generalized biomass equations for North American
634 tree species. Forestry 87:129–151.

635 Cole DM (1977) Protecting and storing increment cores in plastic straws [Research techniques, Pinus
636 contorta latifolia]. Research Note INT-US Dept. of Agriculture

637 Cook ER (1985) A Time Series Analysis Approach to Tree Ring Standardization.

638 Cook ER, Peters K (1997) Calculating unbiased tree-ring indices for the study of climatic and environmental
639 change. holocene 7:361–370.

640 Cook ER, Woodhouse CA, Eakin CM, et al (2004) Long-term aridity changes in the western United States.
641 Science 306:1015–1018.

642 Coop JD, Givnish TJ (2007) Spatial and temporal patterns of recent forest encroachment in montane
643 grasslands of the Valles Caldera, New Mexico, USA. J Biogeography 34:914–927.

644 Daniels LD, Dobry J, Klinka K, Feller MC (1997) Determining year of death of logs and snags of Thuja plicata
645 in southwestern coastal British Columbia. Can J For Res 27:1132–1141.

646 Davis SC, Hessl AE, Scott CJ, Adams MB (2009) Forest carbon sequestration changes in response to timber
647 harvest. Forest Ecology and … 258:2101–2109.

648 Douglass AE (1941) Crossdating in dendrochronology. Journal of Forestry 39:825–831.

649 Dye A, Barker Plotkin A, Bishop D, et al (2016) Comparing tree-ring and permanent plot estimates of
650 aboveground net primary production in three eastern U.S. forests. Ecosphere 7.

651 Eisen K, Plotkin AB (2015) Forty years of forest measurements support steadily increasing aboveground
652 biomass in a maturing, Quercus-dominant northeastern forest. The Journal of the Torrey Botanical
653 Society 142:97–112.

654 Esper J, Niederer R, Bebi P, Frank D (2008) Climate signal age effects—Evidence from young and old trees
655 in the Swiss Engadin. Forest Ecology and Management 255:3783–3789.

656 Finkral AJ, Evans AM (2008) The effects of a thinning treatment on carbon stocks in a northern Arizona
657 ponderosa pine forest. Forest Ecology and Management 255:2743–2750.

658 Fisher R, McDowell N, Purves D, et al (2010) Assessing uncertainties in a second-generation dynamic
659 vegetation model caused by ecological scale limitations. New Phytologist 187:666–681.

660 Foster DR (1988) Disturbance History, Community Organization and Vegetation Dynamics of the Old-
661 Growth Pisgah Forest, South-Western New Hampshire, U.S.A. J Ecology 76:105–134.

662 Foster JR, Finley AO, D'Amato AW, et al (2016) Predicting tree biomass growth in the temperate–boreal
663 ecotone: Is tree size, age, competition, or climate response most important? Glob Change Biol 2138–
664 2151.

665 Friedlingstein P, Cox P, Betts R, et al (2006) Climate-carbon cycle feedback analysis: Results from the
666 C4MIP model intercomparison. Journal of Geophysical Resaerch: Biogeosciences 19:3337–3353.

667 Graumlich LJ, Brubaker LB, Grier CC (1989) Long-Term Trends in Forest Net Primary Productivity: Cascade
668 Mountains, Washington. Ecology 70:405.

669 Griffin D, Meko DM, Touchan R, et al (2011) Latewood Chronology Development for Summer-Moisture
670 Reconstruction in the Us Southwest. Tree-Ring Research 67:87–101.

671 Griffin D, Woodhouse CA, Meko DM, et al (2013) North American monsoon precipitation reconstructed
672 from tree-ring latewood. Geophys Res Lett 40:954–958.

673 Grissino-Mayer HD (2001) Evaluating crossdating accuracy: a manual and tutorial for the computer
674 program COFECHA. Tree-Ring Research 57:205–221.

675 Holmes RL (1983) Computer-assisted quality control in tree-ring dating and measurement. Tree-ring
676 bulletin 43:69–78.

677 Jenkins JC, Chojnacky DC, Heath LS, Birdsey RA (2004) Comprehensive database of diameter-based
678 biomass regressions for North American tree species. US Department of Agriculture, Forest Service,
679 Newtown Square, PA

680 Kaye JP, Hart SC, Fulé PZ, et al (2005) Initial carbon, nitrogen, and phosphorus fluxes following ponderosa
681 pine restoration treatments. Ecology Letters 15:1581 - 1593.

682 Keenan TF, Carbone MS, Reichstein M, Richardson AD (2011) The model–data fusion pitfall: assuming
683 certainty in an uncertain world. Oecologia 167:587–597.

684 Kerhoulas LP, Kolb TE, Koch GW (2013) Tree size, stand density, and the source of water used across
685 seasons by ponderosa pine in northern Arizona. Forest Ecology and Management 289:425–433.

686 Ketterings QM, Coe R, van Noordwijk M, et al (2001) Reducing uncertainty in the use of allometric biomass
687 equations for predicting above-ground tree biomass in mixed secondary forests. Forest Ecology and
688 Management 146:199–209.

689 Kovács B, Tinya F, Ódor P (2017) Stand structural drivers of microclimate in mature temperate mixed
690 forests. Agricultural and Forest Meteorology 234-235:11–21.

691 Lapenis AG, Lawrence GB, Heim A, et al (2013) Climate warming shifts carbon allocation from stemwood
692 to roots in calcium-depleted spruce forests. Global Biogeochem Cycles 27:101–107.

693 LeBauer DS, Wang D, Richter KT, et al (2013) Facilitating feedbacks between field measurements and
694 ecosystem models. Ecological Monographs 83:133–154.

695 Lenoir J, Hattab T, Pierre G (2017) Climatic microrefugia under anthropogenic climate change: implications
696 for species redistribution. Ecography 40:253–266.

697 Lorimer CG, Frelich LE (1989) A methodology for estimating canopy disturbance frequency and intensity in
698 dense temperate forests. Canadian Journal of Forest … 19:651–663.

699 Lu M, Zhou X, Yang Q, et al (2012) Responses of ecosystem carbon cycle to experimental warming: a meta-
700 analysis. Ecology 121113202315001.

701 Mackenzie DI, Royle JA (2005) Designing occupancy studies: general advice and allocating survey effort.
702 Journal of Applied Ecology 42:1105–1114.

703 Mann ME, Bradley RS, Hughes MK (1998) Global-scale temperature patterns and climate forcing over the
704 past six centuries. Nature 392:779–787.

705 Nehrbass-Ahles C, Babst F, Klesse S, et al (2014) The influence of sampling design on tree-ring-based
706 quantification of forest growth. Global Change Biology 20:2867–2885.

707 Nickless A, Scholes RJ, Archibald S (2011) A method for calculating the variance and confidence intervals
708 for tree biomass estimates obtained from allometric equations. South African Journal of Science
709 107:86–95.

710 Pacala SW, Canham CD, Saponara J, et al (1996) Forest models defined by field measurements: Estimation,
711 error analysis and dynamics. Ecological Monographs 66:1–43.

712 Pederson N, Dyer JM, McEwan RW (2014) The legacy of episodic climatic events in shaping temperate,
713 broadleaf forests. Ecological Monographs 84:599–620.

714 Poulter B, Frank D, Ciais P, et al (2014) Contribution of semi-arid ecosystems to interannual variability of
715 the global carbon cycle. Nature 509:600–603.

716 Richardson AD, Williams M, Hollinger DY, et al (2010) Estimating parameters of a forest ecosystem C
717 model with measurements of stocks and fluxes as joint constraints. Oecologia 164:25–40.

718 Rollinson CR, Kaye MW, Canham CD (2016) Interspecific variation in growth responses to climate
719 and competition of five eastern tree species. Ecology 97:1003–1011.

720 Rubino DL, McCarthy BC (2004) Comparative analysis of dendroecological methods used to assess
721 disturbance events. Dendrochronologia 21:97–115.

722 Shaver GR, Canadell J, CHAPIN FS III, et al (2000) Global warming and terrestrial ecosystems: a conceptual
723 framework for analysis. BioScience 50:871–882.

724 Speer, JH (2010) Fundamentals of Tree-Ring Research. U. of Arizona Press, Tucson, Arizona.

725 St George S (2014) An overview of tree-ring width records across the Northern Hemisphere. Quaternary
726 Science Reviews 95:132–150.

727 St George S, Ault TR (2014) The imprint of climate within Northern Hemisphere trees. Quaternary Science
728 Reviews 89:1–4.

729 St George S, Meko DM, Cook ER (2010) The seasonality of precipitation signals embedded within the North
730 American Drought Atlas. The Holocene 20:983–988.

731 Stokes, M. A. , and T. L. Smiley (1968) An introduction to tree-ring dating. University of Chicago Press,
732 Chicago, Illinois, USA.

733 Swetnam TW, Allen CD, Betancourt JL (1999) Applied Historical Ecology: Using the Past to Manage for the
734 Future. Ecological Applications 9:1189–1206.

735 Swetnam TW, Lynch AM (1989) A tree-ring reconstruction of western spruce budworm history in the
736 southern Rocky Mountains. Forest science 35:962–986.

737 Touchan R, Allen CD, Swetnam TW (1996) Fire history and climatic patterns in ponderosa pine and mixed-
738 conifer forests of the Jemez Mountains, northern New Mexico.

739 Touchan R, Woodhouse CA, Meko DM, Allen C (2011) Millennial precipitation reconstruction for the Jemez
740 Mountains, New Mexico, reveals changing drought signal. Int J Climatol 31:896–906.

741 van Mantgem PJ, Stephenson NL, Byrne JC, et al (2009) Widespread Increase of Tree Mortality Rates in the
742 Western United States. Science 323:521–524.

743 Weiner J (2004) Allocation, plasticity and allometry in plants. Perspectives in Plant Ecology, Evolution and
744 Systematics 6:207–215.

745 Williams AP, Allen CD, Macalady AK, Griffin D (2012) Temperature as a potent driver of regional forest
746 drought stress and tree mortality.

747 Wigley T, Briffa K, Jones P (1984) On the average value of correlated time series, with applications in
748 dendroclimatology and hydrometeorology. Journal of Climate and Applied Meteorology 23:201–213.

749 Wood SN (2011) Fast stable restricted maximum likelihood and marginal likelihood estimation of
750 semiparametric generalized linear models. Journal of the Royal Statistical Society: Series B (Statistical
751 Methodology) 73:3–36.

752 Wood SN (2004) Stable and Efficient Multiple Smoothing Parameter Estimation for Generalized Additive
753 Models. Journal of the American Statistical Association 99:673–686.

754 Yamaguchi DK (2011) A simple method for cross-dating increment cores from living trees. Can J For Res
755 21:414–416.

756 Yee TW, Mitchell ND (1991) Generalized additive models in plant ecology. Journal of Vegetation Science
757 2:587–602.

758 (2012) Temperature as a potent driver of regional forest drought stress and tree mortality. 2:1–6.

759

760

Supplemental Material

Table S1. Sample size and dating success at both the plot- and the site-level for an upper elevation spruce dominated forest (Upper Site) and a lower elevation ponderosa pine dominated forest (Lower Site) in the Valles Caldera, NM. Gap filled trees were simulated with generalized additive mixed model to reduce any potential bias from missing trees.

Site	Plot	# Cored trees	Crossdated	Undated	Gap filled
Upper Site		101	77	2	22
	Plot A	50	35	0	15
	Plot B	51	42	2	7
Lower Site		100	86	11	3
	Plot A	50	41	6	3
	Plot B	50	45	5	0

Table S2. Tree-ring chronology statistics for dated cores at both the Upper and Lower Sites in the Valles Caldera, NM. Start date refers to the oldest tree in the chronology, and End Date indicates the year of sampling. Rbar corresponds to the mean between-tree correlation, and the Interseries correlation is based upon all core samples. The Expressed Population Signal (EPS) is a measure of how well the signal recorded in the sampled trees reflects the population signal (Wigley et al. 1984).

Site	Plot	Start Date	End Date	Length (yrs)	Rbar	Interseries Correlation	EPS
Upper Site		1923	2011	88	0.574	0.708	0.961
	Plot A	1924	2011	87	0.581	0.713	0.923
	Plot B	1923	2011	88	0.591	0.720	0.934
Lower Site		1929	2011	82	0.666	0.755	0.975
	Plot A	1935	2011	76	0.713	0.788	0.959
	Plot B	1929	2011	82	0.642	0.735	0.949

Table S3. References for allometric equations that were used to calculate the 'allometric uncertainty'. Jenkins et al. (2004) and Chojnacky et al. (2013) publications house specific parameter values and equation forms for allometric equations used in this analysis.

Site	Common Name	Reference
Lower Site	*Pinus ponderosa*	modified Chojnacky et al 2013*
Lower Site	*Populus tremuloides*	Campbell et al. 1985
Lower Site	*Populus tremuloides*	Campbell et al. 1985
Lower Site	*Populus tremuloides*	Campbell et al. 1985
Lower Site	*Populus tremuloides*	Campbell et al. 1985
Lower Site	*Populus tremuloides*	Freedman et al. 1982
Lower Site	*Populus tremuloides*	Johnston and Bartos 1977
Lower Site	*Populus tremuloides*	Ker 1980
Lower Site	*Populus tremuloides*	Ker 1984
Lower Site	*Populus tremuloides*	Lieffers and Campbell 1984
Lower Site	*Populus tremuloides*	Maclean and Wein 1976
Lower Site	*Populus tremuloides*	Pastor et al. 1984
Lower Site	*Populus tremuloides*	Pastor and Bockheim 1981
Lower Site	*Populus tremuloides*	Peterson et al. 1970
Lower Site	*Populus tremuloides*	Pollard 1972
Lower Site	*Populus tremuloides*	Pollard 1972
Lower Site	*Populus tremuloides*	Pollard 1972
Lower Site	*Populus tremuloides*	Ruark and Bockheim 1988
Lower Site	*Populus tremuloides*	Singh 1984
Lower Site	*Populus tremuloides*	Singh 1984
Lower Site	*Populus tremuloides*	Young et al. 1980
Lower Site	*Populus tremuloides*	Young et al. 1980
Upper Site	*Picea* sp.	Chojnacky et al. 2013
Upper Site	*Picea* sp.	Young et al. 1980
Upper Site	*Pseudotsuga menzesii*	Barclay et al. 1986
Upper Site	*Pseudotsuga menzesii*	Barclay et al. 1986
Upper Site	*Pseudotsuga menzesii*	Barclay et al. 1986
Upper Site	*Pseudotsuga menzesii*	Barclay et al. 1986

*Equation derived from Chojnacky et al. 2013, Personal comm. Chojnacky Feb 2015

Equation form 3 Jenkins et al. 2004: $\ln(\text{biomass}) = -3.5185 + 2.6909 * \ln(\text{DBH})$

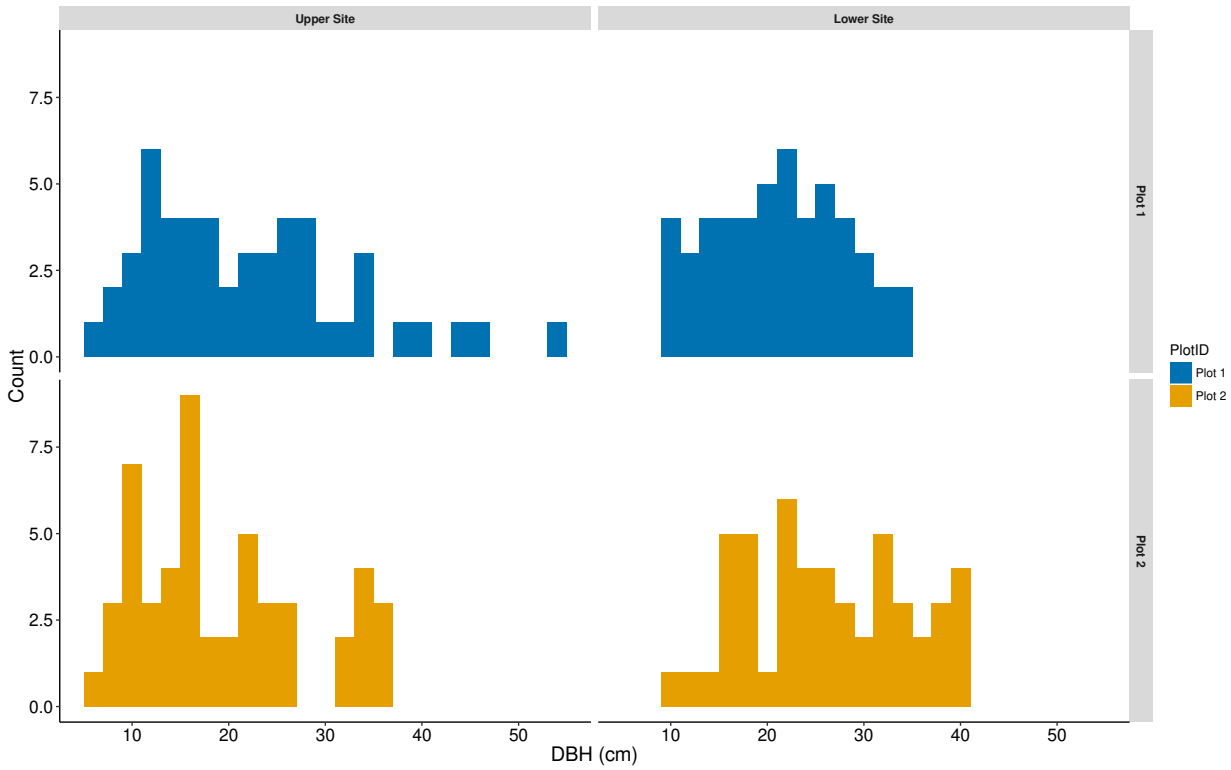

Supplemental Figure 1. Histograms of diameters (DBH) of trees from two sites in the Valles Caldera that were sampled in this study and used to reconstruct biomass at these sites.

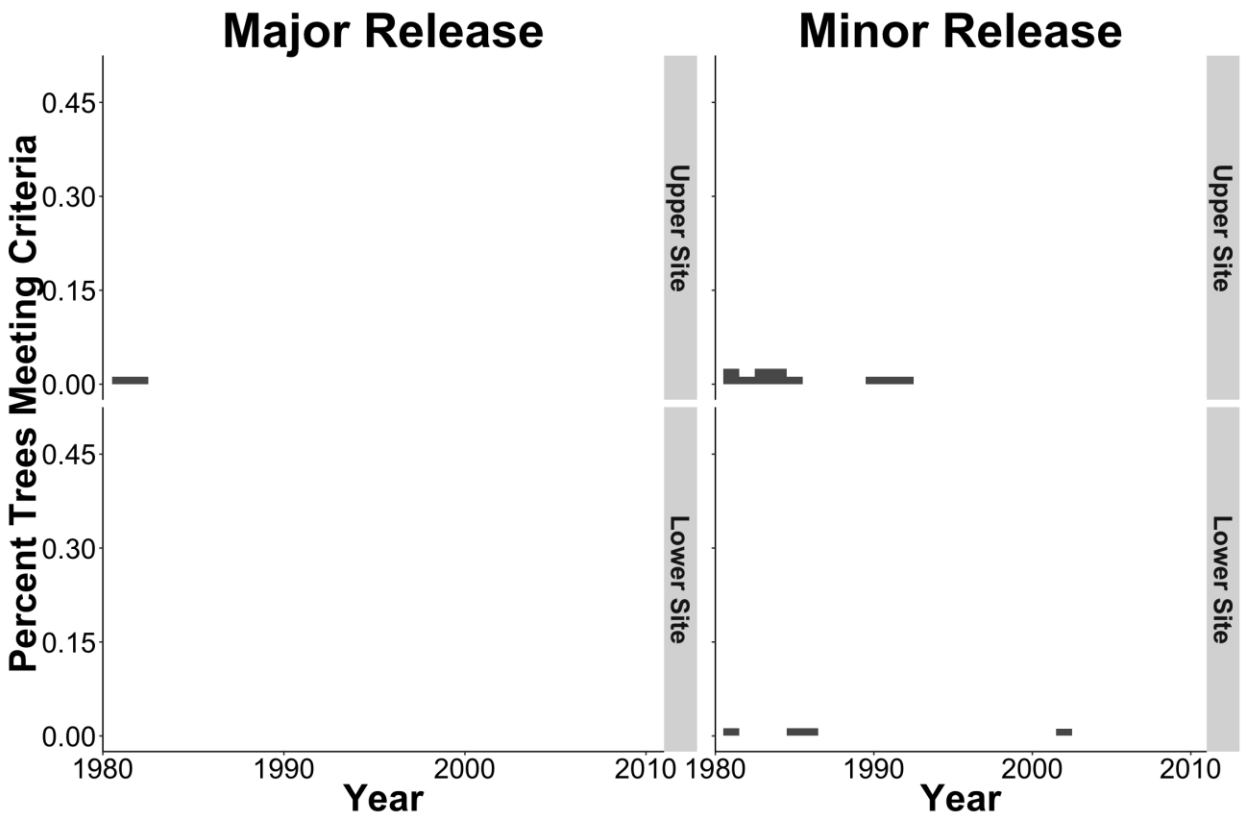

787

788 **Supplemental Figure 2.** Major and minor release analysis events for both the Upper and Lower Sites at the
789 Valles Caldera, NM. Definitions of major and minor events adheres to criteria proposed in Lorimer and
790 Frelich (1989), and no significant, synchronous, major release events are detected for the period of 1980-
791 2011 at either the Upper Site (<3% of sampled trees) or Lower Site (0% of sampled trees) in this study.

792

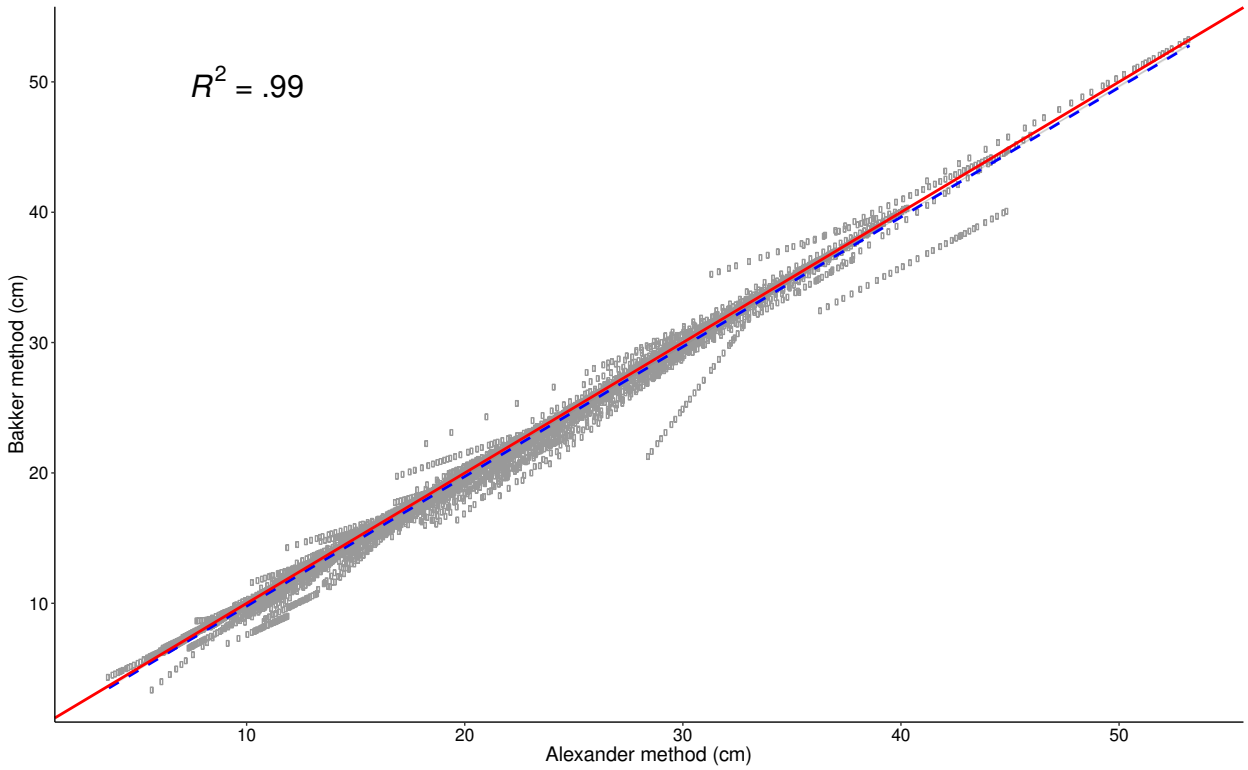

Supplemental Figure 3. Comparison between the diameter reconstruction (DBH) that we employed in our study (Davis et al. 2009; Dye et al. 2016) with the proportional diameter reconstruction methodology outlined in (Bakker 2005). The Solid red line is the 1:1 line and the dashed blue line is the best fit line through the data. For the period of 1980-2011 the two methods produce similar results, producing an R^2 value of 0.99, and a y-intercept of 0.32 cm.

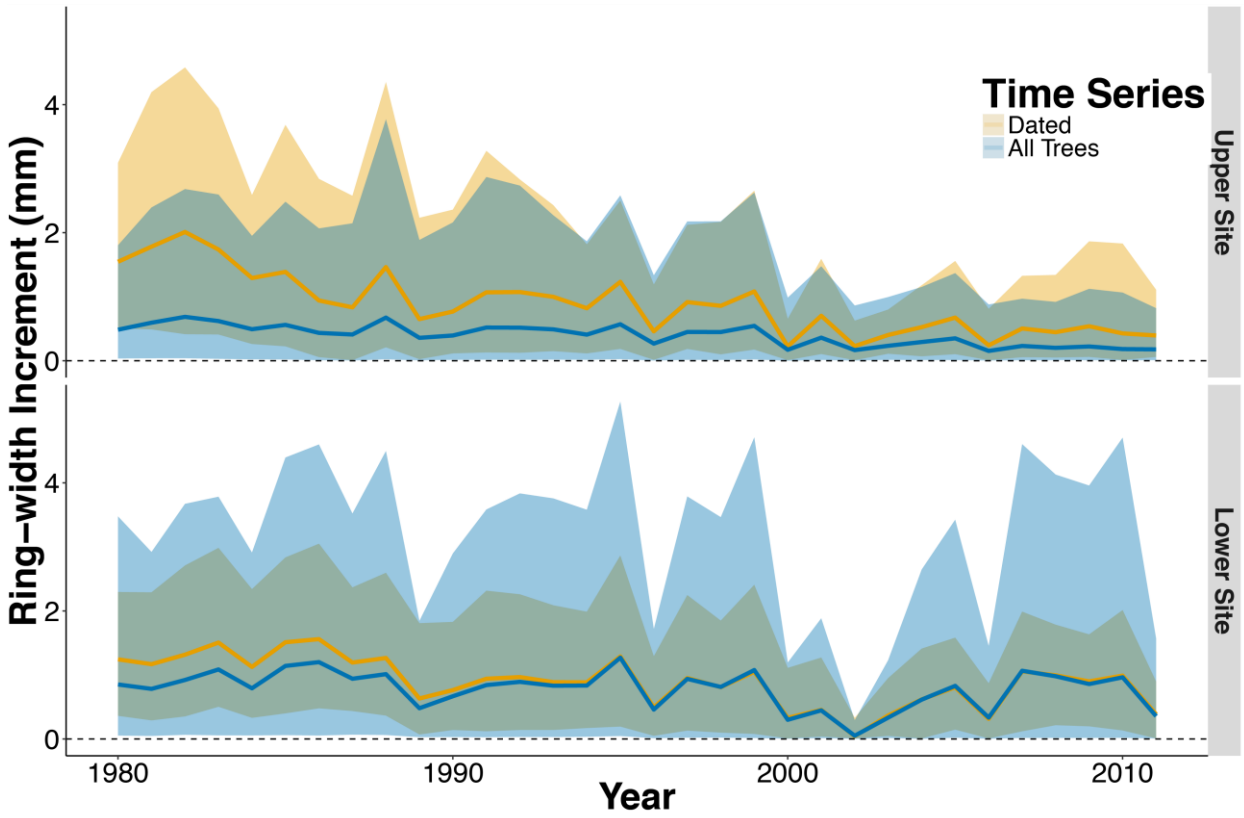

Supplemental Figure 4. Two time series for samples collected at the Valles Caldera, NM. The 'Dated' time series (orange) is composed of only trees that met visual and statistical crossdating standards. The 'All Trees' time series (blue) contains both dated samples and gap filled samples. The mean ring width (mm; line) for each site is accompanied by the 95% CI (shaded area).

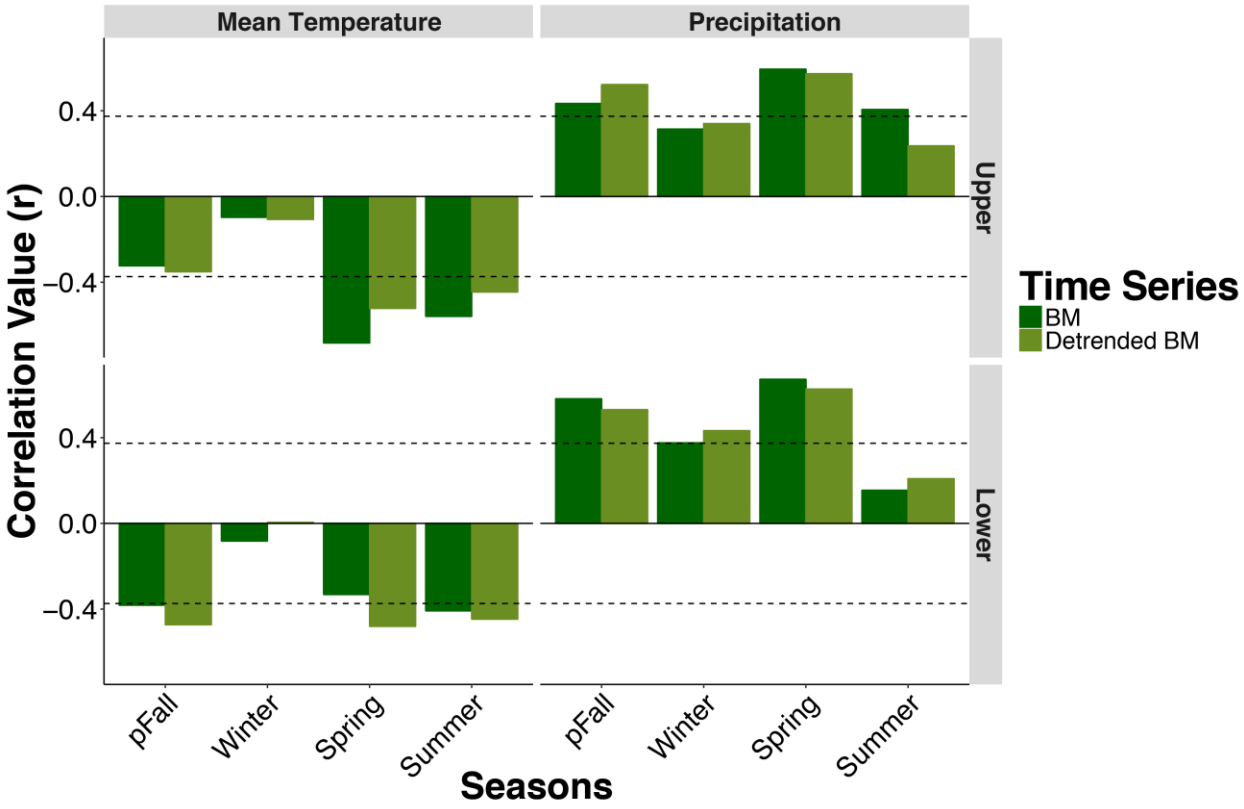

Supplemental Figure 5. Seasonal (pFall = previous Sept., Oct., Nov.; Winter = previous Dec., current Jan, Feb.; Spring = Mar., Apr., May; Summer = Jun, July, Aug.) growth-climate response of the raw mean biomass estimate (BM) and the detrended mean biomass estimate with mean temperature and precipitation (sum; PRISM Climate Group 2004) at an upper elevation (Upper) and a lower elevation (Lower) site in the Valles Caldera, NM. Bold colors indicate a significant ($\alpha = 0.05$) relationship. The growth-climate response is similar between the two time series, and therefore only the BM time series is used in the manuscript.

Figure 1

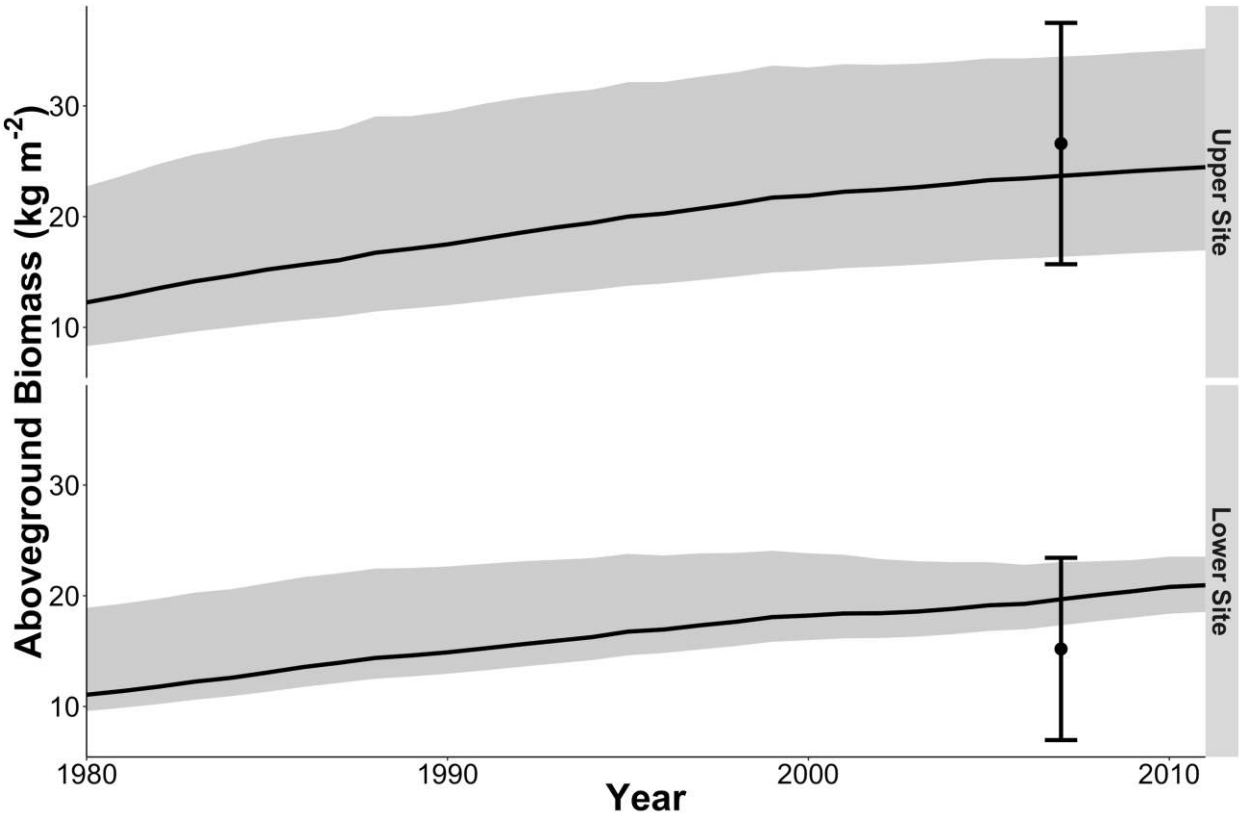

Figure 1. Site-level cumulative biomass estimates with total uncertainty ranges for an upper elevation Engelmann spruce dominated (Upper Site) and lower elevation ponderosa pine dominated forest (Lower Site) at the Valles Caldera, NM. The dark black line represents the mean cumulative biomass estimate traditionally reported, and the shaded grey area is the 95% CI of biomass from adding all sources of uncertainty together in quadrature. Points and error bars represent an independent assessment (Mean ± 1.96*SD; n = 4) of living biomass (assuming a 50% carbon content) from 2007 for both sites (Anderson-Teixeira et al. 2011).

Figure 2

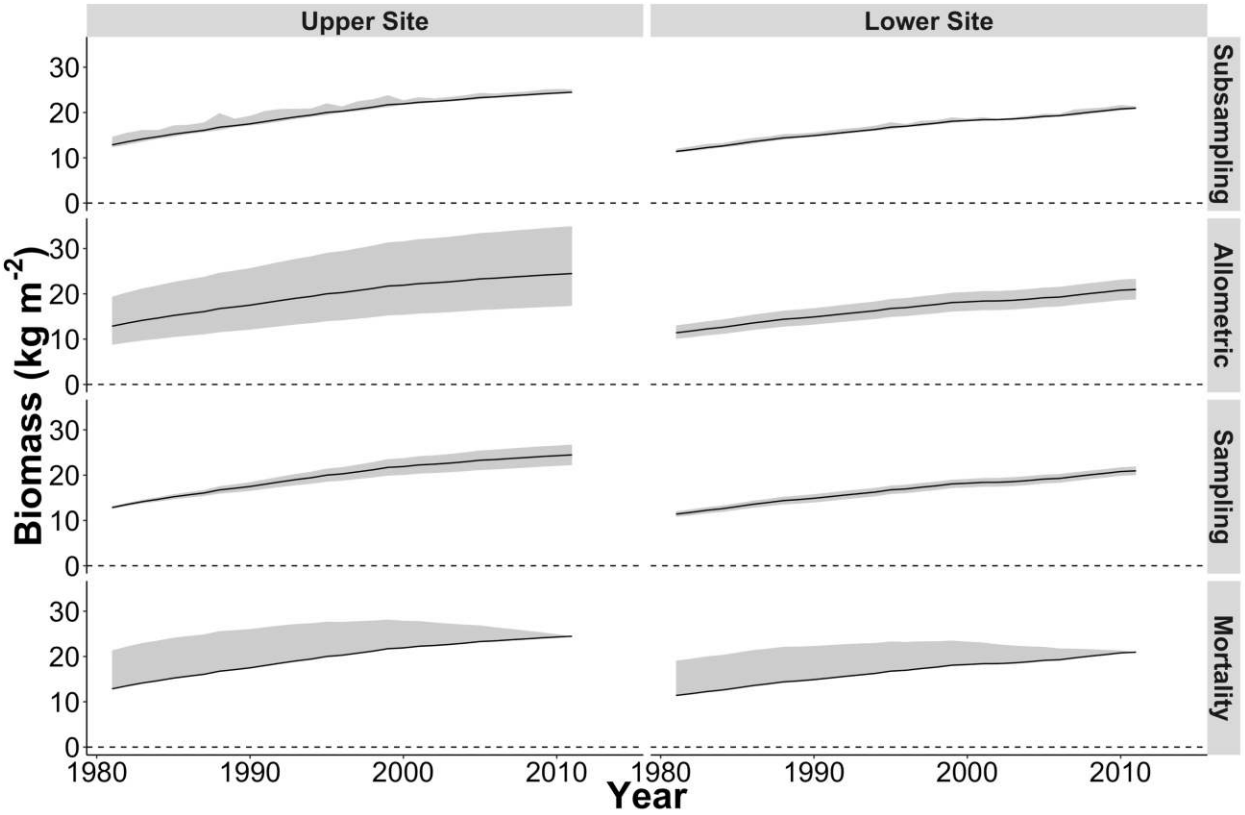

Figure 2. Cumulative tree-ring derived biomass estimates for the Upper Site (left column) and the Lower Site (right column) at the Valles Caldera. The black line represents the biomass calculated for the mean allometric equation for each site, and the shaded area is the 95% confidence interval for each source of uncertainty.

Figure 3

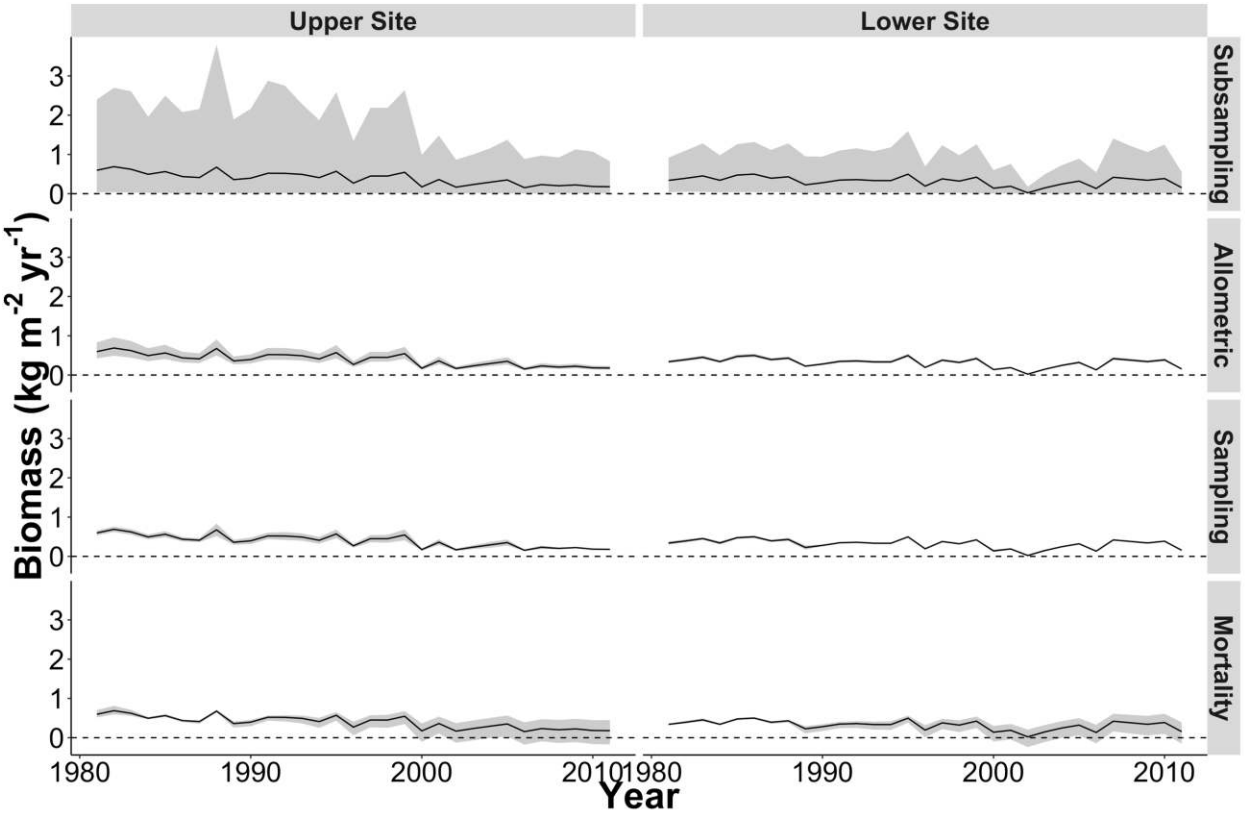

Figure 3. Interannual tree-ring derived biomass estimates for the Upper Site (left column) and the Lower Site (right column) at the Valles Caldera. The black line represents the mean interannual biomass increment calculated for each site, and the shaded area is the 95% confidence interval for each source of uncertainty.

Figure 4

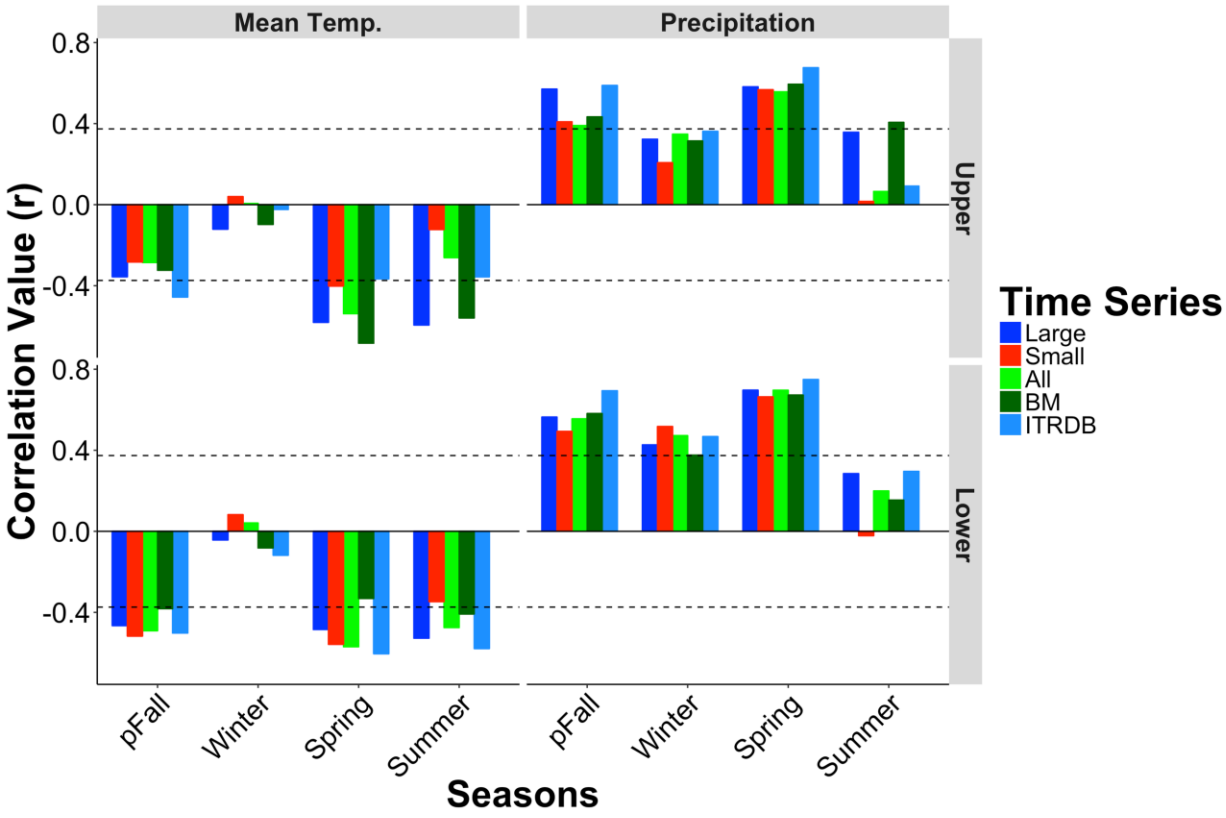

Figure 4. Seasonal (previous Fall, Winter, Spring, Summer) growth-climate response of mean biomass increment estimates (dark green) and four tree-ring chronologies (Large, Small, All, ITRDB) with mean temperature and total precipitation at an upper (Upper Site) and a lower (Lower Site) elevation site in the Valles Caldera, NM. The Large chronology (blue) is composed of the largest 10% of trees by DBH and the Small chronology (red) is composed of the smallest 10%. The ITRDB chronology (light blue) was gathered from ITRDB (Upper Site: Touchan et al. 2011; Lower Site: Brice et al. 2013). The mean biomass increment time series (light green) represents the mean annual biomass increment for each site. Significant responses were identified as those values exceeding the ($\alpha = 0.05$) significance criterion (dashed line).

Figure 5

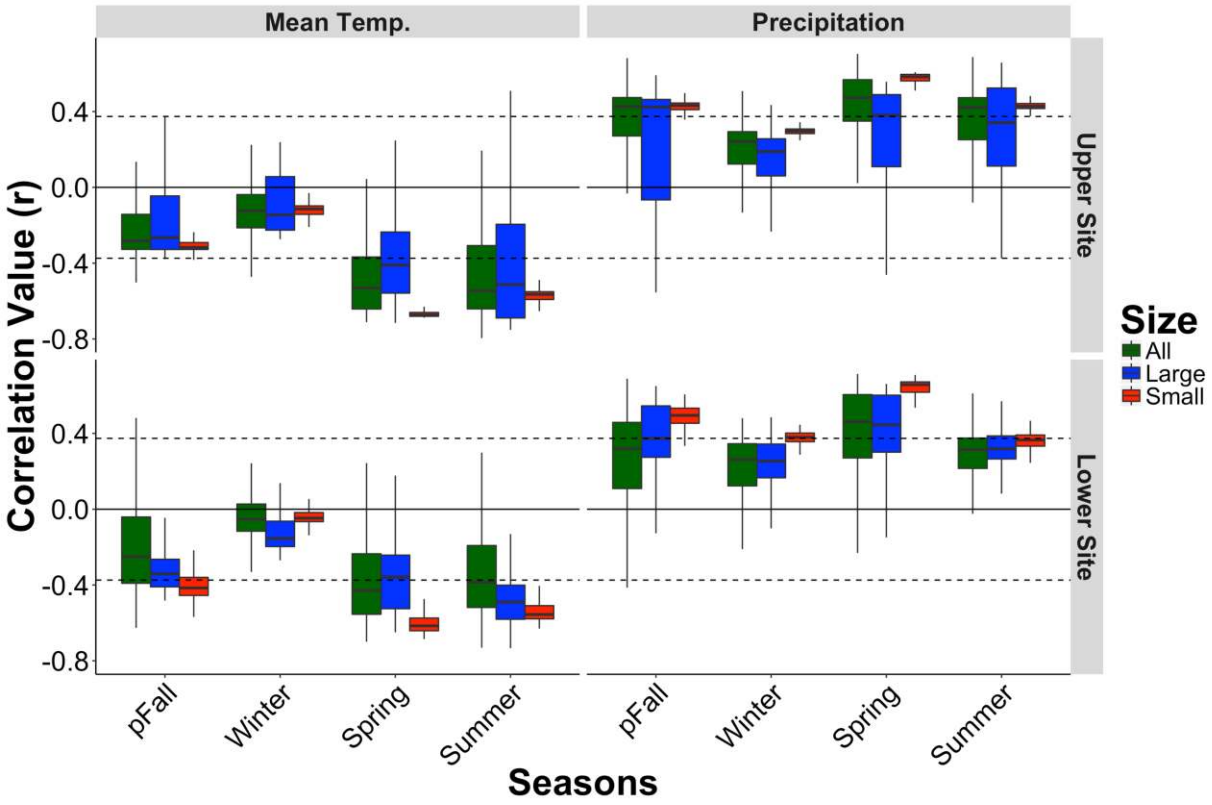

Figure 5. Distributions of growth-climate relationships for simulated biomass time series from an upper elevation (Upper Site; PIEN) and a lower elevation (Lower Site; PIPO) forest in the Valles Caldera, NM. The Large time series is based on the largest 10% of trees, the Small time series is based on the smallest 10% of trees, and the All time series is composed of all trees sampled. Distributions were generated by bootstrapping, with replacement, 30,000 time series meeting each of the three criteria and performing a Pearson's correlation analysis. Solid bars refer to the mean r-value.

Table 1. Mean ± SD for cumulative and incremental living aboveground biomass uncertainty ranges (kg m^{-2}) for 1980 – 2011 of major sources of variability at an upper elevation and a lower elevation forest in the Valles Caldera, NM. Total uncertainty is calculated by adding the upper and lower 95% confidence intervals of each area of uncertainty in quadrature.

Source	Cumulative Range (kg BM m^{-2})		Incremental Range (kg BM $m^{-2}y^{-1}$)	
	Upper Site	Lower Site	Upper Site	Lower Site
Allometric	14.88 ± 2.14	3.89 ± 0.47	0.20 ± 0.09	0.15 ± 0.06
Subsampling	1.84 ± 0.76	0.98 ± 0.30	1.84 ± 0.76	3.19 ± 1.25
Sampling	2.86 ± 1.35	1.78 ± 0.21	0.13 ± 0.07	0.85 ± 0.36
Mortality	6.39 ± 2.82	5.39 ± 2.50	0.30 ± 0.19	0.61 ± 0.40
Total	17.67 ± 0.93	8.15 ± 1.73	1.95 ± 0.70	1.06 ± 0.25

Response to reviewer

Click here to access/download

Electronic Supplementary Material

Sept2017_reponse_to_reviewers(2).docx

Supplemental Figure 1

Click here to access/download

Electronic Supplementary Material

Supplemental Figure 1.docx

Supplemental Figure 2

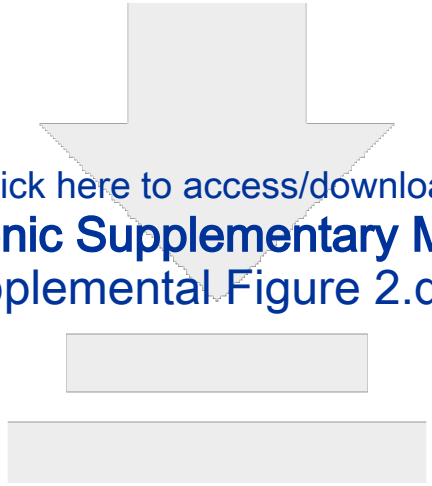

Click here to access/download

Electronic Supplementary Material

Supplemental Figure 2.docx

Supplemental Figure 3

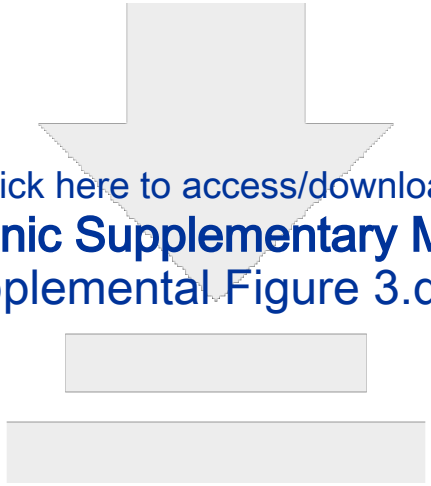

Click here to access/download

Electronic Supplementary Material

Supplemental Figure 3.docx

Supplemental Figure 4

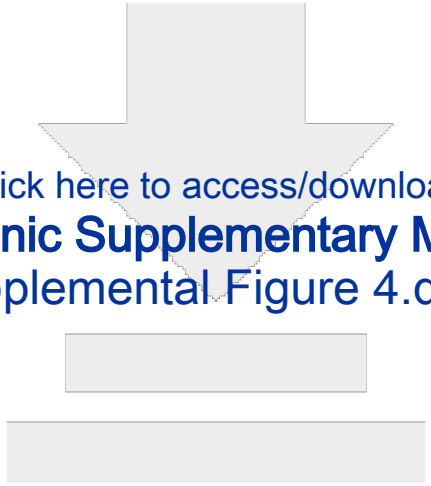

Click here to access/download

Electronic Supplementary Material

Supplemental Figure 4.docx

Supplemental Figure 5

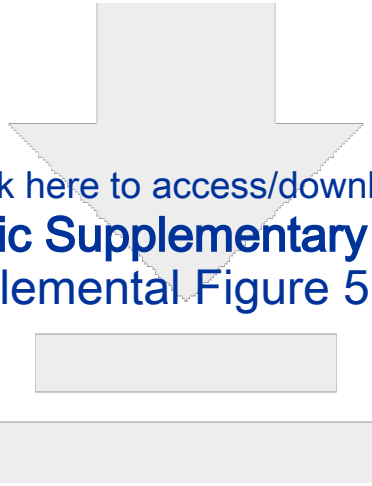

Click here to access/download

Electronic Supplementary Material

Supplemental Figure 5.docx

Table S1

Click here to access/download

Electronic Supplementary Material

Table S1.docx

Table S2

Click here to access/download

Electronic Supplementary Material

Table S2.docx

Table S3

Click here to access/download

Electronic Supplementary Material

Table S3.docx